Mineral Equilibrium Constraints on the Feasibility of Diffusively-Fluxed Melting in the Continental Crust

Lorena Andrea Tafur

a dissertation submitted in fulfilment of the degree of

Master of Science

in the Department of Geological Sciences,

University of Cape Town, South Africa.

February 2019

Plagiarism Declaration

I, Lorena Andrea Tafur (Student number: TFRLOR002), know the meaning of plagiarism and declare that all of the work in the dissertation (or thesis), save for that which is properly acknowledged, is my own.

Signature: Signed by candidate Date: 11.02.2019

Abstract

Generation of granitic magma predominantly occurs by melting through the breakdown of hydrous minerals. However, melting due to the influx of water has been recognised in anatectic amphibolite-facies composite grey gneisses, metagreywackes and low-pressure metapelites, and has consequently been proposed as an alternative mechanism for granite generation and crustal differentiation. Water-fluxed melting is recognised by voluminous melt production at relatively low temperature, where hydrous minerals are stable and anhydrous minerals are preferentially consumed during melting. Mineral equilibrium modelling to determine the P–T conditions, melt volumes, melting reactions and viable fluid sources reveal that water-present melting in all target lithologies is confined to the wet solidus and does not extend to temperatures higher than 700–710 °C. Melting at suprasolidus conditions does not involve the mechanical flow of a free water phase. Instead, the process is driven by diffusion of H_2O along chemical potential gradients and is therefore more appropriately described as diffusively-fluxed melting. Diffusively-fluxed melting is not restricted to specific compositions or P–T conditions, although it is more efficient at lower pressure and in lithologies with a low hydrous mineral content. Melting reactions in all lithologies primarily consume quartz and feldspars to yield 5–6 mol.% melt for each mol.% of H_2O added. a_{H_2O} remains constant at ∼0.70–0.77 during progressive melting as long as alkali feldspar is present. Once alkali feldspar is exhausted, plagioclase becomes the main reagent, producing more tonalitic melt compositions with gradually higher a_{H_2O}. Melting will initiate and proceed as long as a μ_{H_2O} gradient exists between the fluid source and target lithology. Our calculations show that an ordinary magma, such as an I-type magma with typical, undersaturated H_2O content, has a μ_{H_2O} high enough to be a viable fluid source, allowing diffusively-fluxed melting to produce melt volumes and fertility comparable to that of dehydration melting. However, voluminous melt production requires a considerable volume of H_2O, which necessitates a focussed fluid source such as a magma conduit or

melt-bearing shear zone. Any other magmatic fluid source will undergo a similar amount of crystallisation as the melt fraction produced in the target rock, such that there will be no net melt production. Considering that shear-zone hosted magma conduits are relatively rare, diffusively-fluxed melting appears to only be viable in a small fraction of the anatectic orogenic crust. Therefore, whereas it may play a significant role in locally raising melt volumes and modifying magma chemistry through mingling and hybridisation, it does not appear to, of itself, be able to meaningfully contribute to crustal differentiation.

Acknowledgements

I would like to express my deep gratitude to Associate Professor Johann Diener, my research supervisor, for his patient guidance, encouragement and valuable support during this research work. Without his motivation, I would not have had the opportunity to share this work with the wider academic community at various conferences, and for this I am truly thankful. I would also like to thank my fellow colleague, Simon Schorn, for his helpful advice and assistance when it came to the modelling work.

I would also like to acknowledge the funding received to support this research from the the National Research Foundation of South Africa (grant 105781). In addition, I would like to thank Kumba Iron Ore Limited for its contribution towards my studies and academic development.

Finally, I must express my very profound gratitude to my family for providing me with unfailing support and continuous encouragement throughout my years of study and through the process of researching and writing this thesis. This accomplishment would not have been possible without them. Thank you.

Lorena Tafur

Contents

List of Tables

List of Figures

Chapter 1

Introduction

The formation of granitic magma by partial melting in the mid- to lower crust and its subsequent migration and emplacement in the upper crust are the most significant processes contributing to crustal differentiation (Clemens & Vielzeuf, 1987; Sandiford & McLaren, 2002; Brown, 2013). Thus, understanding the formation and thermal evolution of continental crust largely relies on a thorough knowledge of the mechanisms and products of partial melting. It is widely accepted that differentiation of the crust is primarily controlled by fluid-absent melting reactions that involve hydrous mineral breakdown (Powell, 1983; Thompson, 1983; Clemens & Vielzeuf, 1987; White *et al.*, 2001; Clemens, 2006; Brown & Korhonen, 2009; Brown, 2013). The alternative—that crustal differentiation is primarliy driven by fluid-present melting reactions, which consume free aqueous fluids—was largely refuted in the 1980s after profuse historical debate (Thompson, 1955; Tuttle & Bowen, 1958; Wyllie, 1977; Turner, 1981; Etheridge *et al.*, 1983; Powell, 1983; Thompson, 1983; Rubie, 1986; Clemens & Vielzeuf, 1987; Berger *et al.*, 2008; Vernon & Clarke, 2008; Brown, 2013).

Until the early 1980s, the classic view of metamorphism in the Earth's crust assumed that a free fluid phase was always present (Tuttle & Bowen, 1958; Norris & Henley, 1976; Turner, 1981), even during partial melting (Wyllie, 1977; Etheridge *et al.*, 1983). However, as new physical, petrological and geochemical arguments developed throughout the decade, the temporal and spatial pervasiveness of free fluid in the crust was challenged (Hoernes & Friedrichsen, 1978; Heinrich, 1982; Walther & Orville, 1982; Thompson, 1983; Yardley & Baltatzis, 1985). It was proposed that free fluids could only be present for limited durations of time, for instance, while dehydration reactions are occurring or during fluid infiltration events (Hoernes & Friedrichsen, 1978; Heinrich, 1982; Walther & Orville, 1982; Thompson, 1983; Yardley & Baltatzis, 1985). The accumulation of a free water phase during these events would also be restricted to definite locations, which on a regional scale, could include massive magma emplacements or shear zones (Thompson, 1983).

Three influential papers published in the mid-1980s (Powell, 1983; Thompson, 1983; Clemens

& Vielzeuf, 1987) seemingly resolved the controversy with the conclusion that fluid-absent melting, otherwise known as dehydration melting, likely characterised partial melting in the lower to mid-crustal regions because: (i) lower to mid-crustal regions have inadequate pore space to hold significant volumes of free fluid necessary for voluminous melt production (Ramberg, 1952; Yardley & Valley, 1997; Yardley, 2009); (ii) water-saturated melts are unable to ascend through the crust, unless segregated from the source (Clemens & Droop, 1998), as decompression results in solidification (Wickham, 1987; Collins *et al.*, 1989; Finger & Clemens, 1995); and (iii) the water-saturated solidus prevents aqueous fluids from accessing supra-solidus terranes (Cartwright *et al.*, 1995). At these conditions, fluids are rapidly consumed to produce melt causing a pressure decrease, which subsequently draws more fluid into the area.

1.1 Evidence for water-fluxed melting

These three principal arguments deemed fluid-present melting as a minor melt-producing process with an insignificant impact on crustal differentiation. Despite this, the role that aqueous fluids may have in crustal melting and the generation of granitic magma has acquired renewed interest, with many now referring to this process as 'water-fluxed' melting (e.g. Weinberg & Hasalová, 2015; Collins *et al.*, 2016; Schwindinger & Weinberg, 2017). A recent review paper by Weinberg & Hasalová (2015) defines water-fluxed melting as synonymous with water-assisted or water-present melting and states that it describes "crustal melting (in) the presence of a free H_2O phase". Weinberg & Hasalová (2015) comprehensively evaluate water-fluxed melting and present numerous natural examples of anatectic terranes where this process is inferred to have occurred. These examples involve instances where the volume of melt observed is greater than that which is expected from dehydration melting, with many case studies using this as evidence to validate the presence of external H_2O during melting. In addition, melting occurred at relatively low temperatures at which dehydration melting is not yet significant, with petrological observations further suggesting that hydrous minerals were not consumed during melting. These examples also include relatively anhydrous lithologies, where voluminous melting is unlikely to have occurred exclusively through dehydration melting (Sawyer, 2010). Prevalent rock types where melting through the addition of fluid has been described include composite grey gneiss complexes (Collins *et al.*, 1989; Mogk, 1992; Pognante, 1992; Nédélec *et al.*, 1993; Sawyer, 1998; Escuder Viruete, 1999; Jung *et al.*, 2000; White *et al.*, 2005; Jung *et al.*, 2009; Sawyer, 2010; Lee & Cho, 2013; Finch *et al.*, 2014; Carvalho *et al.*, 2016; Wu *et al.*, 2018), metagreywackes (Brown, 1979; Milord *et al.*, 2001; Fornelli *et al.*, 2002; Genier *et al.*, 2008; Schwindinger & Weinberg, 2017) and low-pressure aluminous metapelites (Wickham & Taylor, 1985; Wickham, 1987; Yardley & Barber, 1991; Ellis & Obata, 1992; Cartwright *et al.*, 1995; Butler *et al.*, 1997; Cartwright & Buick, 1998; Ward *et al.*, 2008; Kisters *et al.*, 2009). Given the diverse range of natural examples, Weinberg & Hasalová (2015) emphasise that melting by fluxing H_2O-rich fluids in

suprasolidus terranes needs to be considered as a viable granite-forming mechanism because it appears to be widespread in diverse tectonic environments.

Weinberg & Hasalová (2015) address known issues with water-fluxed melting and suggest potential fluid sources, fluid pathways into suprasolidus terranes, and characteristics of the magma produced by this process. Considering the very low pore space of the mid- to lower crust, fluids would have to be externally sourced and likely channelised into the rocks undergoing melting. Proposed mid-crustal fluid sources are either deformation-driven metamorphic reactions in shear zones (Mogk, 1992; Sawyer, 2010) or crystallising magma intrusions (Huppert & Sparks, 1988; Collins *et al.*, 1989; Yardley & Barber, 1991; Finger & Clemens, 1995; Annen & Sparks, 2002; Berger *et al.*, 2008; Weinberg & Hasalová, 2015). These fluids still need to overcome water-saturated conditions in the crust, where aqueous fluids are rapidly consumed at the wet solidus, posing an issue for water-fluxed melting in suprasolidus terranes (Cartwright *et al.*, 1995). Overcoming this natural barrier could be accomplished through the direct transportation of aqueous fluids into suprasolidus terranes by focussed fluid channels such as shear zones and fractures (Mogk, 1992; Sawyer, 2010). Alternatively, fluid may be transported by water-rich magmas migrating up-temperature in regions of inverted geothermal gradient, such as orogenic thrust fronts (e.g. Le Fort *et al.*, 1987; Holk & Taylor, 2000; Berger *et al.*, 2008; Hasalová *et al.*, 2008; Sawyer, 2010; Finch *et al.*, 2014), or by lateral or downward migration due to tectonic pressure gradients (e.g. Cartwright *et al.*, 1995).

In all of these mechanisms, the aqueous fluid or hydrous melt promotes melting by fluxing in an effort to achieve equilibrium with the relatively dry surroundings (Weinberg & Hasalová, 2015). This recognises the possible role that water-activity gradients around fluid sources have in driving partial melting in suprasolidus terranes (White & Powell, 2010; Weinberg & Hasalová, 2015). In a rock-buffered environment where there is a limited volume of fluid, the intial fluid influx temporarily and locally raises the water-activity of the system, however P–T conditions ultimately govern the water-acitivity at which the system equilbrates (Weinberg & Hasalová, 2015). Therefore, this process involving free aqueous fluids in suprasolidus conditions could generate water-undersaturated melts capable of rising through the crust (Clemens & Vielzeuf, 1987; Clemens & Droop, 1998) and potentially produce Cordilleran-type batholiths (Collins *et al.*, 2016). This would suggest that magmas generated by water-fluxed melting reactions have an influence in continental evolution and could therefore explain part of the diverse range of granitoids, in addition to some anomalous features of many anatectic terranes (Weinberg & Hasalová, 2015; Collins *et al.*, 2016).

1.2 Arguments against water-fluxed melting

These ideas are not widely accepted and have been challenged by Clemens & Stevens (2015), among others. In a response to Weinberg & Hasalová (2015), Clemens & Stevens (2015) emphasises that even though magmas generated in water-fluxed conditions could be water-

undersaturated and consequently upward mobile (Clemens & Droop, 1998), the composition of the majority of crustally-derived magmas indicate they were formed by high-temperature, fluid-absent partial melting reactions. Furthermore, experiments have shown dehydration melting can adequately account for the observed volumes and compositions of felsic igneous rocks emplaced in the crust (Clemens & Vielzeuf, 1987; Johannes & Holtz, 1996; Clemens & Droop, 1998; Clemens, 2006). Metamorphic conditions recorded by mineral assemblages in anatectic granulite terranes are also associated with dehydration melting. Thus, dehydration melting is a particularly simple mechanism for producing magmas, and it can neatly explain observations on the composition and structure of the continental crust (Clemens & Stevens, 2015). Ultimately, Clemens & Stevens (2015) argued that water-fluxed melting is an unnecessarily complicated solution for regional crustal differentiation and is a minor process limited by available fluid volume (Stevens & Clemens, 1993).

Despite these objections, the numerous case studies reviewed by Weinberg & Hasalová (2015) demonstrate that water-fluxed melting can occur in nature and is a potentially important petrogenetic process, but it has not been made clear under what exact conditions it is possible, what the requirements and limitations are for its feasibility, and whether the process is general and fertile enough to ultimately contribute to crustal differentiation.

1.3 Objectives for this thesis

In this thesis, I use mineral equilibrium modelling and calculated chemical potential gradients to test the feasibility of water-fluxed melting for typical crustal lithologies where the process has been proposed, namely composite grey gneiss complexes, metagreywackes and low-pressure aluminous metapelites. This technique is capable of modelling the predicted behaviour of rocks and fluids during water-fluxed melting, and has the potential to provide insights into the conditions under which it may be a feasible petrogenetic process.

Note that, whereas Weinberg & Hasalová (2015), Collins *et al.* (2016), Schwindinger & Weinberg (2017) and others have termed this process 'water-fluxed melting', I will rather refer to it as 'diffusively-fluxed melting' in this thesis. This is to highlight that the process is driven by diffusion along chemical potential gradients rather than the mechanical flow of water, as will be explained in upcoming chapters. Furthermore, whereas H_2O will be the only mobile component considered here, diffusively-fluxed melting can equally encompass open-system fluxing by any other mobile component (such as O_2, Na_2O or K_2O; cf. Korzhinskiĭ, 1959; Münster, 1970; Carlson, 2002). Throughout upcoming chapters, the term fluid will be used to refer to an aqueous-rich fluid that unless explicitly stated to be a 'free' fluid, is not considered as a physically-distinct separable phase. Water is reserved for instances when fluid is physically present, whereas H_2O is used to distinguish the component irrespective of its physical state.

Case studies of carefully documented natural examples where diffusively-fluxed melting is

proposed will be used to validate the modelling of representative compositions of the typical crustal lithologies. This thesis will ultimately investigate the likely P–T conditions of melting, calculate the volume of melt that can be generated, identify the main melting reactions, and test the viability of proposed fluid sources.

Chapter 2

Selected Case Studies

2.1 Archaean composite grey gneiss complexes

Key observations associated with diffusively-fluxed melting—low melting temperature, anhydrous bulk mineralogy and the survival of hydrous minerals—are documented in some composite grey gneiss complexes (Collins *et al.*, 1989; Mogk, 1992; Pognante, 1992; Nédélec *et al.*, 1993; Sawyer, 1998; Escuder Viruete, 1999; Jung *et al.*, 2000; White *et al.*, 2005; Jung *et al.*, 2009; Sawyer, 2010; Lee & Cho, 2013; Finch *et al.*, 2014; Carvalho *et al.*, 2016; Wu *et al.*, 2018). These are therefore important examples of diffusively-fluxed melting, especially because composite grey gneisses are the predominant lithological units in high-grade gneiss terranes in Archaean continental crust (White *et al.*, 2017). The term 'composite grey gneiss' describes a terrane dominated by tectonically intermingled intermediate to felsic rocks, which may also contain fragments of mafic to ultramafic components (Moyen, 2011; White *et al.*, 2017). For the purpose of this thesis, 'composite grey gneiss' exclusively describes the predominant granitoid component of these terranes, which is compositionally dominated by tonalitic-trondhjemitic-granodioritic (TTG) gneiss (Moyen, 2011; White *et al.*, 2017). This thesis examines two natural examples of Archaean composite grey gneiss terranes (Figs. 2.1) that are documented to have undergone amphibolite-facies diffusively-fluxed melting (Sawyer, 2010; Carvalho *et al.*, 2016). The study of Sawyer (2010) describes melting of leucogranodiorite and leucotonalite from the Neoarchaean Opatica Subprovince of the Superior Province in the Canadian Shield (Fig.2.2a), whereas Carvalho *et al.* (2016) describes melting of leucogranodiorite in the Kinawa migmatites of the Campo Belo Metamorphic Complex in the southern part of the Mesoarchaean–Palaeoproterozoic São Francisco Craton in Brazil (Fig.2.2b). Both terranes experienced regional deformation associated with migmatisation, as predominant north-vergent back thrusts occur in the area of the Opatica migmatites (Sawyer, 2010) and the Kinawa migmatites are associated with a large regional shear zone that has reworked the Archaean TTG crust (Carvalho *et al.*, 2016).

A notable feature of composite grey gneisses is that they are dominated by plagioclase feldspar

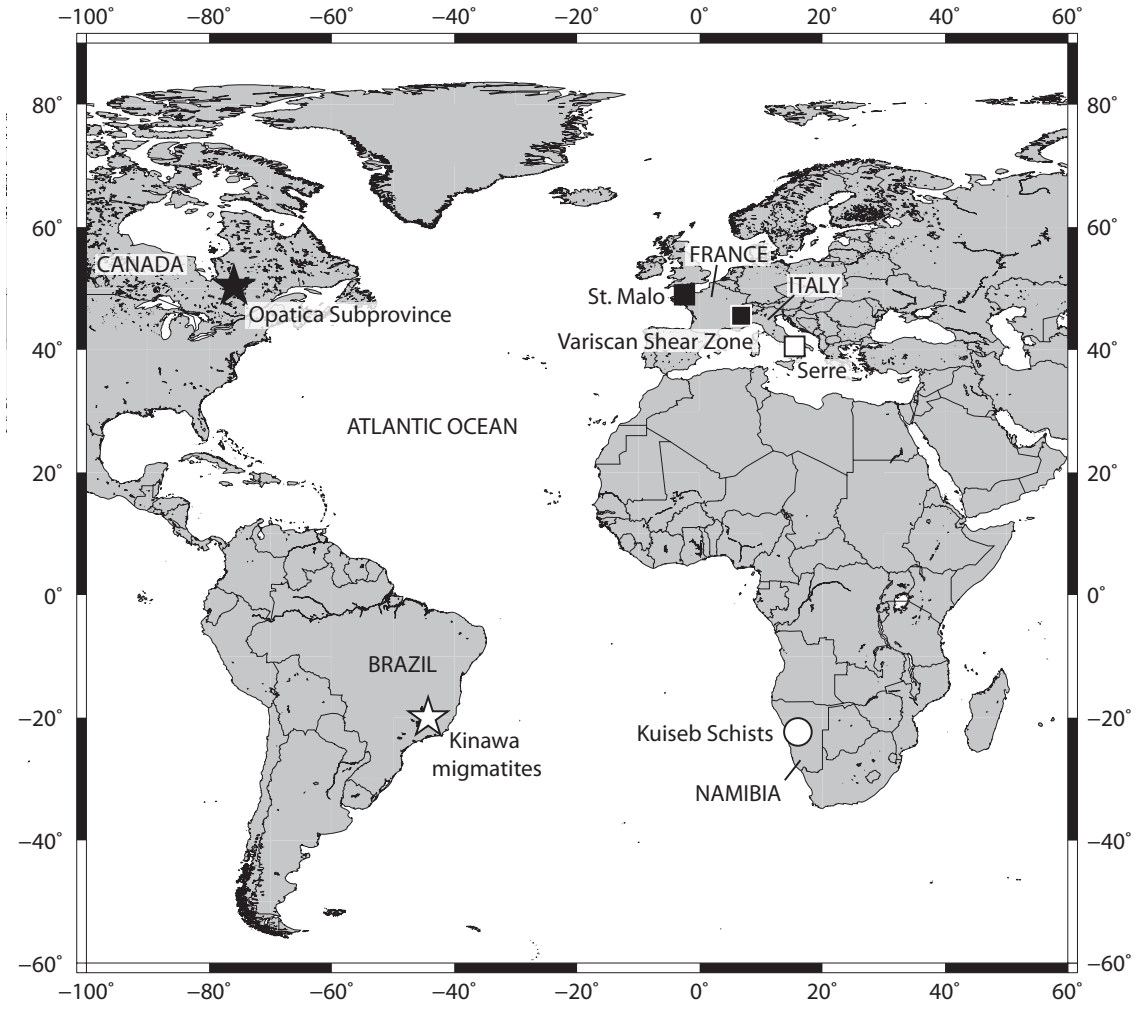

Figure 2.1: World map showing the approximate locations of the selected case studies: the Opatica Subprovince, Superior Province; the Kinawa migmatites of the São Franciso Craton; the Variscan Shear Zone in the Aiguilles-Rouges massif; the Serre, Southern Italy; the St. Malo Terrane of the Armorican massif; and the Kuiseb Schists of the Damara Sequence.

and can either contain minor quantities of K-feldspar or be K-feldspar depleted (Moyen, 2011). This is reflected in the protolith assemblages of the Opatica and Kinawa migmatites, which both consist of large quantities of quartz ($\sim$ 30%) and plagioclase ($\sim$ 40–60%) along with a low abundance of K-feldspar ($<$ 20%) and minor amounts of biotite ($<$ 7%); this highlights the relatively anhydrous nature of composite grey gneisses (Sawyer, 2010; Carvalho *et al.*, 2016). The Kinawa protolith contains a maximum of 20% K-feldspar (Carvalho *et al.*, 2016) and the Opatica protolith contains an average of 9.4% K-feldspar (Sawyer, 2010). Consequently, the more K-feldspar rich leucogranodiorite protolith of the Kinawa migmatites has the potential to produce more melt than the leucogranodiorite and leucotonalite protolith of the Opatica migmatites. Accessory phases comprise 1.2% of the Opatica protolith, and these include epidote, magnetite, ilmenite, titanite, apatite, zircon and monazite (Sawyer, 2010). The

Kinawa protolith assemblage consists of less than 1% accessory phases, which are apatite, allanite, zircon and magnetite (Carvalho *et al.*, 2016).

Partial melting in these migmatitic terranes occurred at peak metamorphic conditions of 730 ± 25 °C and 5–6 kbar. These conditions and related uncertainties were calculated by Sawyer (2010) and Carvalho *et al.* (2016) using a combination of well-established thermobarometers. The relatively low peak metamorphic temperature is one of few potential indicators that suggest dehydration melting is not responsible for the observed large volumes of anatectic granites in the Opatica and Kinawa migmatite terranes (Sawyer, 1998).

Biotite is the main hydrous mineral in these composite grey gneiss protoliths and if dehydration melting had occurred, it would have been preferentially consumed. Unexpectedly, the biotite in these protoliths appears to be unaffected by melting, which is inferred from its straight, well-defined grain boundaries and relatively constant abundance (Sawyer, 2010; Carvalho *et al.*, 2016). Instead, the residual rocks in the Opatica Subprovince show a decrease in abundance of quartz and microcline and an increase in plagioclase and biotite (Sawyer, 2010). A similar observation is made in the residual rocks of the Kinawa migmatites, where K-feldspar depletion is coupled with enrichment in plagioclase, quartz, biotite and accessory phases relative to the protolith (Carvalho *et al.*, 2016). Other than its apparent stability, biotite also exists in very low quantities in the leucogranodiorite protoliths of these terranes. This means, even if entirely consumed, biotite would be an insufficient hydrous source for dehydration melting reactions to generate the voluminous melts observed (Sawyer, 1998, 2010; Carvalho *et al.*, 2016). Thus, the following fluid-present melting reaction was proposed for these composite grey gneisses:

$$\mathrm{K-feldspar} + \mathrm{quartz} + \mathrm{plagioclase} + \mathrm{H_2O} = \mathrm{melt} \tag{2.1}$$

where K-feldspar is observed to be the limiting reactant (Sawyer, 2010; Carvalho *et al.*, 2016).

Mass balance calculations indicate 25–30% partial melting occurred in the Opatica Subprovince (Sawyer, 2010). For the Kinawa migmatites, geochemical modelling indicates 35–40% partial melting occurred (Carvalho *et al.*, 2016). However, given the Kinawa protolith has a maximum K-feldspar content of 20%, a maximum of 60% melt could have been produced (Carvalho *et al.*, 2016). Both regions contain rocks that are K-feldspar depleted, indicating that the proposed melting reaction went to completion. Importantly, this would suggest that the melting reaction was not limited by the availability of H_2O, which contradicts the comment made by Clemens & Stevens (2015). These case studies used oxygen isotopes to suggest that the external aqueous fluid, which induced melting was either metamorphic in origin or released from a crystallising magma in the case of the Kinawa migmatites (Sawyer, 2010; Carvalho *et al.*, 2016). Shear zones in these terranes are the proposed pathways for the aqueous fluid (Sawyer, 2010; Carvalho *et al.*, 2016).

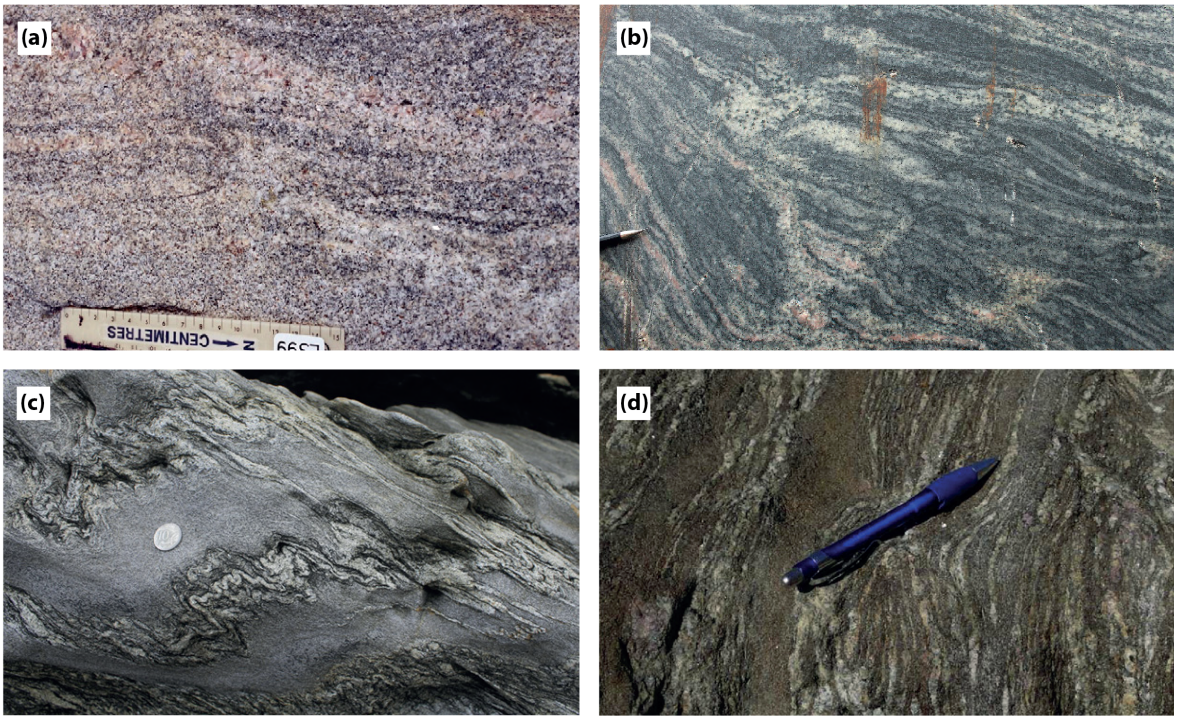

Figure 2.2: Field photographs taken from selected case studies. (a) Metatexite migmatite from the Opatica Subprovince in the Canadian Shield [Taken from Sawyer (2010, Fig. 3b)]. (b) Grey metatexite from the Kinawa migmatite of the Campo Belo Metamorphic Complex in the São Francisco Craton [Taken from Carvalho *et al.* (2016, Fig. 2b)]. (c) Metatexite formed from partially melted Kanmantoo metasedimentary rocks in the Stun'Sail Boom River area on Kangaroo Island [Taken from Schwindinger & Weinberg (2017, Fig. 2b)]. (d) Stromatic leucosome with new generations of cordierite and garnet found in Kuiseb Schists of the Damara Belt [Taken from Ward *et al.* (2008, Fig. 3b)].

2.2 Metagreywackes

Metagreywackes have also been considered as suitable candidates for diffusively-fluxed melting (Brown, 1979; Milord *et al.*, 2001; Fornelli *et al.*, 2002; Genier *et al.*, 2008; Schwindinger & Weinberg, 2017). This is because of the predominantly anhydrous mineralogy of metagreywackes and the interbedded clay-rich sediments, which are suggested to be the fluid source for diffusively-fluxed melting. Unlike other lithologies where diffusively-fluxed melting is proposed, there is significant compositional variability among the metagreywackes which introduces some variability regarding protolith mineralogy, partial melting conditions, reactions and associated melting features. Therefore, no specific example is used to validate the modelling, instead common observations from all case studies are considered for a general case of diffusively-fluxed melting in the metagreywackes (Fig.2.1). Among the case studies considered by Weinberg & Hasalová (2015), protolith mineralogies are not specifically identified, although metagreywackes that have undergone negligible partial melting are commonly described to be dominated by quartz and plagioclase with varying amounts of biotite (Table 2.1; Brown, 1979; Milord *et al.*, 2001; Fornelli *et al.*, 2002; Genier *et al.*, 2008; Schwindinger & Weinberg, 2017). Some variation between these 'protolith' assemblages is the presence or absence of minor amounts of muscovite, garnet or sillimanite.

The conditions of partial melting for the metagreywacke examples encompass a large range of P–T conditions, with the only limitation being temperature as this does not exceed 800 °C (Table 2.1). Metagreywackes from the St. Malo terrane of the Armorican massif in France are estimated to undergo partial melting at temperatures less than 800 °C and at pressures between 4–7 kbar (Milord *et al.*, 2001). Genier *et al.* (2008) proposes lower P–T conditions of 630–670 °C at 2–4 kbar for metagreywackes from the Variscan Shear Zone of the Aiguilles-Rouges massif in the western Alps. Whereas, in the Serre of Southern Italy, partial melting is estimated to have occurred at 700–800 °C at 5–8 kbar (Fornelli *et al.*, 2002). Most recently, Schwindinger & Weinberg (2017) describes partial melting of metasedimentary rocks at Kangaroo Island located on the Adelaide Fold Belt to have occurred between 680–740 °C at pressure conditions below 4.5 kbar (Fig. 2.2c)

Considering the variability of P–T conditions and protolith compositions, melting features are not consistently described, but typically involve the consumption of quartz and plagioclase and muscovite, if present. However, the low temperature of metamorphism, low abundance of muscovite and the scarcity of peritectic minerals associated with muscovite breakdown suggests that the large amount of melt produced is not exclusively attributed to muscovite-dehydration melting (Milord *et al.*, 2001; Fornelli *et al.*, 2002; Schwindinger & Weinberg, 2017). Additionally, biotite is reported across all case studies to be unaffected by melting. Therefore the most frequently suggested melting reactions are 2.1 and

$$\text{muscovite} + \text{quartz} + \text{plagioclase} + \text{H}_2\text{O} = \text{melt} \tag{2.2}$$

The estimated melt volumes for diffusively-fluxed melting in metagreywackes range considerably from lower volumes of 9–13 mol.% in the Serre of Southern Italy (Fornelli *et al.*, 2002) and 20 mol.% melt in the Variscan Shear Zone of the Aiguilles-Rouges massif (Genier *et al.*, 2008), to considerably higher proportions such as the 40 mol.% melt estimated by Milord *et al.* (2001) for metasedimentary rocks of the St. Malo terrane.

2.3 Low-pressure aluminous metapelites

Low-pressure aluminous metapelites offer another example where diffusively-fluxed melting has been regularly proposed (Wickham & Taylor, 1985; Wickham, 1987; Yardley & Barber, 1991; Ellis & Obata, 1992; Cartwright *et al.*, 1995; Butler *et al.*, 1997; Cartwright & Buick, 1998; Ward *et al.*, 2008; Kisters *et al.*, 2009). Compared to composite grey gneisses and metagreywackes, metapelites have a greater abundance of hydrous minerals such as muscovite and biotite. Thus, at low P–T conditions, aluminous metapelites are still susceptible to voluminous melting through the breakdown of muscovite. Diffusively-fluxed melting is therefore principally distinguished by a discrepancy between observed volume of melt compared to the volume expected from dehydration melting reactions (Weinberg & Hasalová, 2015).

This discrepancy, along with other detailed petrological and field constraints for melting is documented for the migmatitic metasedimentary rocks of the Pan-African Damara Belt in Namibia (Fig. 2.1) studied by Ward *et al.* (2008). Ward *et al.* (2008) described metapelitic cordierite-biotite gneisses, which are the predominant rock type of the Kuiseb Formation in the Damara Sequence (Fig. 2.2d). The gneisses are characterised by a solid mineral assemblage consisting of cordierite + biotite + plagioclase + quartz ± K-feldspar ± garnet (± ilmenite). The likely protolith composition would be that of a low-grade schist in the region, in which there are no new generations of garnet and/or cordierite. Peritectic cordierite is distinguished by its nucleation on pre-existing cordierite crystals within the surrounding gneiss, and peritectic garnet is identified within the fracture sites (Ward *et al.*, 2008). Garnet is generally absent in rocks that have not undergone melting (Ward *et al.*, 2008).

Cordierite and/or garnet are peritectic phases linked with incongruent fluid-present melting (Weinberg & Hasalová, 2015); however, this is not the main argument made by Ward *et al.* (2008) for this mechanism. Instead, their argument revolved around the large quantity of melt produced ($\sim$ 10%) for a relatively low-temperature, low-pressure metapelite with no evidence of having undergone muscovite-dehydration melting. Ward *et al.* (2008) refined the peak metamorphic conditions by applying optimal thermobarometry (Powell & Holland, 2008) to the anatectic mineral assemblage, which yielded low-temperature, amphibolite-facies peak conditions of 700–750 °C and 5 ± 1 kbar. This suggests that fluid-absent biotite melting is unlikely to have occured as the accepted onset temperature for this reaction is typically above 800 °C. In addition, partial melting features are localised in dilation sites, creating the possibility that melting involved a free aqueous fluid and was therefore controlled by

fluid availability (Ward *et al.*, 2008). Thus, melting was suggested to have occurred via the incongruent biotite melting reaction:

$$\text{biotite} + \text{quartz} + \text{plagioclase} + \text{H}_2\text{O} = \text{melt} + \text{garnet} + \text{cordierite}. \quad (2.3)$$

This melting reaction was reproduced by experimental data presented by Ward *et al.* (2008) for fluid-absent and water-fluxed partial melting. Possible fluid sources or pathways were not proposed.

Table 2.1: Summary of the selected case studies considered for the modelling

	'Protolith' mineral assemblage	*P–T* conditions	Proposed melting reaction	Melt %
Opatica grey gneiss [a]	pl (58.2%), q (26.8%) Ksp (9.4%), bi (4.4%)	720 ± 30 °C, 5.2–6.2 kbar	$K-feldspar + quartz + plagioclase + H_2O = melt$ (2.1)	25–30
Kinawa grey gneiss[b]	pl (40%), q (30%, Ksp (20%), bi (7%)	727 ± 25 °C, 5.1–6.1 kbar	$K-feldspar + quartz + plagioclase + H_2O = melt$ (2.1)	35–40
Kangaroo Island metagreywackes[c]	q (30–38%), pl (25%), bi (24–28%), Ksp (0–5%)	680–740 °C, 3.5–4.5 kbar	$K-feldspar + quartz + plagioclase + H_2O = melt$ (2.1) or $muscovite + quartz + plagioclase + H_2O = melt$ (2.2)	–
Variscan metagreywackes[d]	bi (30–40%), q (25–30%), Ksp (20–25%), pl (10–20%), mu (0–10%), g (0–10%)	630–670 °C, 2–4 kbar	$K-feldspar + quartz + plagioclase + H_2O = melt$ (2.1)	20
Serre metagreywackes[e]	g, sill, pl, q ± bi	700–800 °C, 5–8 kbar	$muscovite + quartz + plagioclase + H_2O = melt$ (2.2)	9–13
St. Malo metagreywackes[f]	mu, bi, pl, q	<800 °C, 4–7 kbar	$muscovite + quartz + plagioclase + H_2O = melt$ (2.2)	<40%
Kuiseb schists[g]	cd, bi, pl, q ± Ksp ± g (± ilm)	700–750 °C, 5 ± 1 kbar	$biotite + quartz + plagioclase + H_2O = melt + garnet + cordierite$ (2.3)	10

Data sources are: [a]Sawyer (2010); [b]Carvalho *et al.* (2016); [c]Schwindinger & Weinberg (2017); [d]Genier *et al.* (2008); [e]Fornelli *et al.* (2002); [f]Milord *et al.* (2001); [g]Ward *et al.* (2008). Abbreviations used described in Chapter 3.

Chapter 3

Modelling Considerations

P–T, T–M_{H_2O} and P–T–μ_{H_2O} phase diagram calculations are performed using THERMOCALC 3.45 (Powell & Holland, 1988, update October 2016) with an updated version of the internally consistent dataset of Holland & Powell (2011, dataset file tc-ds63.txt, created May 2015) in the MnO–Na_2O–CaO-K_2O–FeO–MgO–Al_2O_3–SiO_2–H_2O–TiO_2–O (MnNCKFMASHTO) chemical system because it is the largest chemical system in which models are currently available. The activity–composition relations used are those of Green *et al.* (2016) for tonalitic melt (L), clinoamphibole (hb), and augitic clinopyroxene (aug). The orthopyroxene (opx), garnet (g), biotite (bi), cordierite (cd), spinel-magnetite (sp-mt) and ilmenite-hematite (ilm-hem) models are from White, Powell & Johnson (2014), whereas the haplogranite melt (liq), muscovite (mu) and feldspar models are from White, Powell, Holland, Johnson & Green (2014). Quartz (q), titanite (sph), sillimanite (sill) and aqueous fluid (H_2O) are treated as pure end-member phases.

3.1 Bulk rock compositions and P–T conditions

To investigate the feasibility of diffusively-fluxed melting in more general terms, representative compositions of typical crustal rocks are required. The average or typical protolith compositions used in the modelling are for two composite grey gneisses, a metagreywacke and an amphibolite-facies metapelite and are presented in Tables 3.1 and 3.2. The disparities between the expected fluid-absent melting evolution of these compositions and the actual melting observations outlined in the case studies (see Section 2) are described using P–T pseudosections presented in Figures 3.1, 3.2 and 3.3.

3.1.1 Composite grey gneiss complexes

Moyen (2011) presented a large compilation of bulk compositions of tonalitic grey gneisses, and the average of this dataset is modelled as the 'tonalitic grey gneiss' composition. A similar dataset was compiled by Garde (1997), but from this dataset the average amphibolite-facies

tonalitic-trondhjemitic-granodioritic (TTG) grey gneiss composition was selected and will be referred to as the 'TTG grey gneiss'. The fluid-absent melting behaviour of both these average compositions was recently described by White *et al.* (2017). Both compositions are tonalitic (see Table 3.1), but show differences with respect to their FeO, MgO, CaO and K_2O content that represents some of the variability in composite grey gneisses. The tonalitic grey gneiss has a relatively higher FeO, MgO and CaO content than the TTG grey gneiss, but contains less K_2O (Table 3.1).

The two chosen compositions are comparable to the case studies from the Opatica Subprovince (Sawyer, 2010) and the Kinawa migmatites (Carvalho *et al.*, 2016). The FeO, MgO, CaO and K_2O variability of the tonalitic and TTG grey gneiss compositions is mirrored by the Opatica and Kinawa migmatites protolith compositions respectively (Table 3.1). The average composite grey gneiss compositions have slightly larger MgO, CaO and smaller K_2O contents than the protoliths of the case studies. There are also some minor discrepancies associated with the Al_2O_3 and Na_2O values (Table 3.1). With respect to the phase equilibria modelling, these small inconsistencies are assumed not to significantly influence the predicted mineral assemblages. Thus, the observations made in the Opatica Subprovince are useful to corroborate the modelling of tonalitic grey gneiss composition (Moyen, 2011), whereas the Kinawa migmatites are suited to validate the modelling of the TTG grey gneiss composition (Garde, 1997).

The conditions of partial melting for these composite grey gneisses are estimated at 730 ± 25 °C and 5–6 kbar (Table 2.1) by Sawyer (2010) and Carvalho *et al.* (2016) and therefore, our modelling of the average composite grey gneiss compositions is conducted at 6 kbar and 750 °C. White *et al.* (2017) conclude that in a closed-system, composite grey gneiss terranes which are fluid-saturated at the solidus, produce very little (5–12 %) melt as partial melting begins in the upper amphibolite-facies (see Fig 3.1). Voluminous melting of these rocks only begins at temperatures in excess of 800–850 °C and is associated with the breakdown of hornblende and/or biotite and growth of orthopyroxene (White *et al.*, 2017). Therefore, under fluid-absent conditions, composite grey gneisses are predicted to produce less than 5 mol.% melt through biotite breakdown at our modelling conditions (Fig. 3.1). Evidently, this is not the case for the Opatica Subprovince and Kinawa migmatites, as these terranes are estimated to have undergone 30–40% partial melting (Sawyer, 2010; Carvalho *et al.*, 2016). Therefore, examples of amphibolite-facies composite grey gneisses with considerably larger melt volumes than predicted, like the Opatica and Kinawa migmatites, are inconsistent with in-situ fluid-absent melting.

3.1.2 Metagreywackes

The average metagreywacke composition selected for this study is the same as that compiled and investigated by Yakymchuk & Brown (2014). Minor manganese (0.2 mol.%) is added to the modelled bulk composition (see Table 3.2), in line with the values reported by Pettijohn

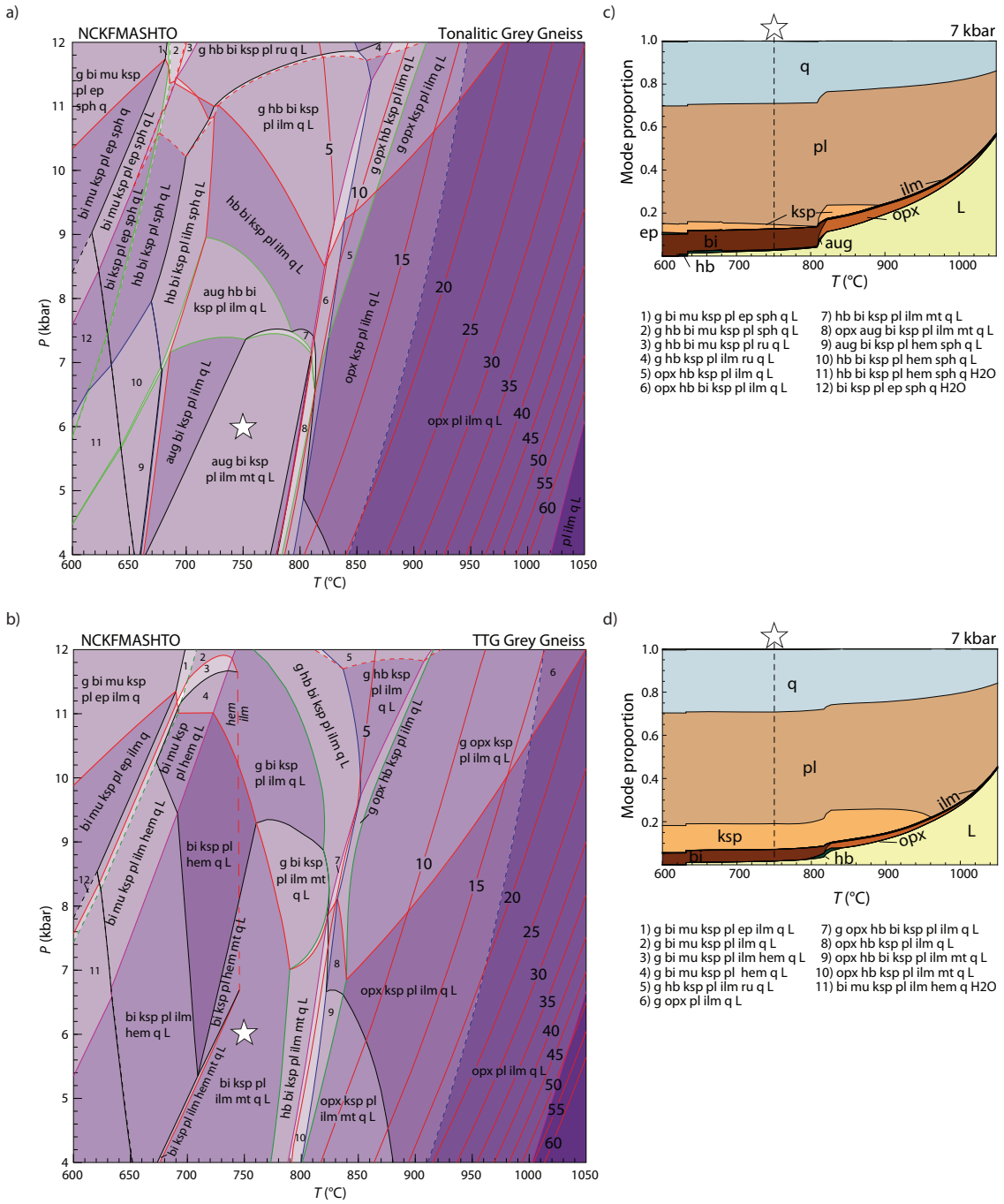

Figure 3.1: *P–T* pseudosections for two average composite grey gneiss compositions including **(a)** the average tonalitic grey gneiss composition of Moyen (2011) and **(b)** the average TTG grey gneiss composition of Garde (1997). Solid red lines indicate contours for the modal proportion of melt. Modebox plots **(c)** and **(d)** show the estimated mineral proportions calculated along an isobaric 7 kbar section through diagrams (a) and (b), respectively. White stars on all diagrams indicate conditions determined by Sawyer (2010) and Carvalho *et al.* (2016) for partial melting. [Modified from White *et al.* (2017, Fig. 5)]

Table 3.1: Major element whole rock data (wt.%) for the average composition of each lithology

	Tonalitic grey gneiss[a]	TTG grey gneiss[b]	Opatica protolith[c]	Kinawa protolith[d]	Passive margin metagreywacke[e]	Kuiseb schist protolith[f]	I-type magma[g]
SiO_2	69.56	71.04	70.81	72.47	70.94	59.75	69.17
TiO_2	0.35	0.25	0.27	0.27	0.63	0.90	0.43
Al_2O_3	15.29	15.48	15.05	14.19	12.72	17.26	14.33
Fe_2O_3	-	0.36	2.33	1.88	5.10	7.67	1.04
FeO	-	1.37	-	-	-	-	2.29
FeO^{tot}	2.66	-	-	-	-	-	-
MnO	0.05	0.03	0.04	0.03	-	0.10	0.07
MgO	1.09	0.57	0.75	0.42	2.35	3.84	1.42
CaO	3.04	2.52	2.90	1.93	0.98	1.16	3.20
Na_2O	4.69	4.71	5.07	3.82	2.68	2.44	3.13
K_2O	1.91	2.65	2.25	3.87	1.81	4.65	3.40
P_2O_5	0.12	0.08	0.10	0.07	-	0.21	0.11
LOI	0.71	0.24	0.43	0.52	2.94	1.58	-
Sum	99.47	99.30	100.00	99.47	100.15	99.56	98.59

Data sources are: [a]Moyen (2011); [b]Garde (1997); [c]Sawyer (2010); [d]Carvalho *et al.* (2016); [e]Yakymchuk & Brown (2014); [f]Ward *et al.* (2008); [g]Whalen *et al.* (1987).

(1963). From the considered case studies of diffusively-fluxed melting in metagreywackes (see Section 2.2), protolith compositions are not identified and an appropriate comparison to the average metagreywacke composition cannot be made. These studies report variable amphibolite-facies P–T conditions with pressures from 2 to 8 kbar and loosely constrained at temperatures below 800 °C (Table 2.1; Brown, 1979; Milord *et al.*, 2001; Fornelli *et al.*, 2002; Genier *et al.*, 2008; Schwindinger & Weinberg, 2017). Given the broad range of conditions, the modelling is conducted at a representative average of 5 kbar and 750 °C.

Notably, our modelling conditions are below those of voluminous melt production which only begins at temperatures in excess of 800 °C and is associated with biotite breakdown and the growth of orthopyroxene and/or K-feldspar (Fig. 3.2a). In a closed system, fluid-saturated metagreywackes are estimated to undergo very little melting at amphibolite-facies conditions, with less than 10% produced. Therefore, case studies of metagreywackes that have produced approximately 10–40% melt at these conditions are unlikely to have experienced fluid-absent melting.

3.1.3 Low-pressure aluminous metapelites

The average amphibolite-facies metapelite composition of Ague (1991) is used in the modelling (Tables 3.1, 3.2), as the phase relations and fluid-absent melting behaviour of this composition has been thoroughly described (e.g. White, Powell, Holland, Johnson & Green, 2014; Yakymchuk & Brown, 2014). Fluid-absent melting occurs primarily through the breakdown of muscovite and biotite at conditions above 4.5 kbar and 700 °C or 780 °C for muscovite- and biotite–sillimanite melting, respectively (e.g. White, Powell, Holland, Johnson & Green, 2014; Yakymchuk & Brown, 2014, see Fig. 3.2b). At conditions below about 4.5 kbar, muscovite

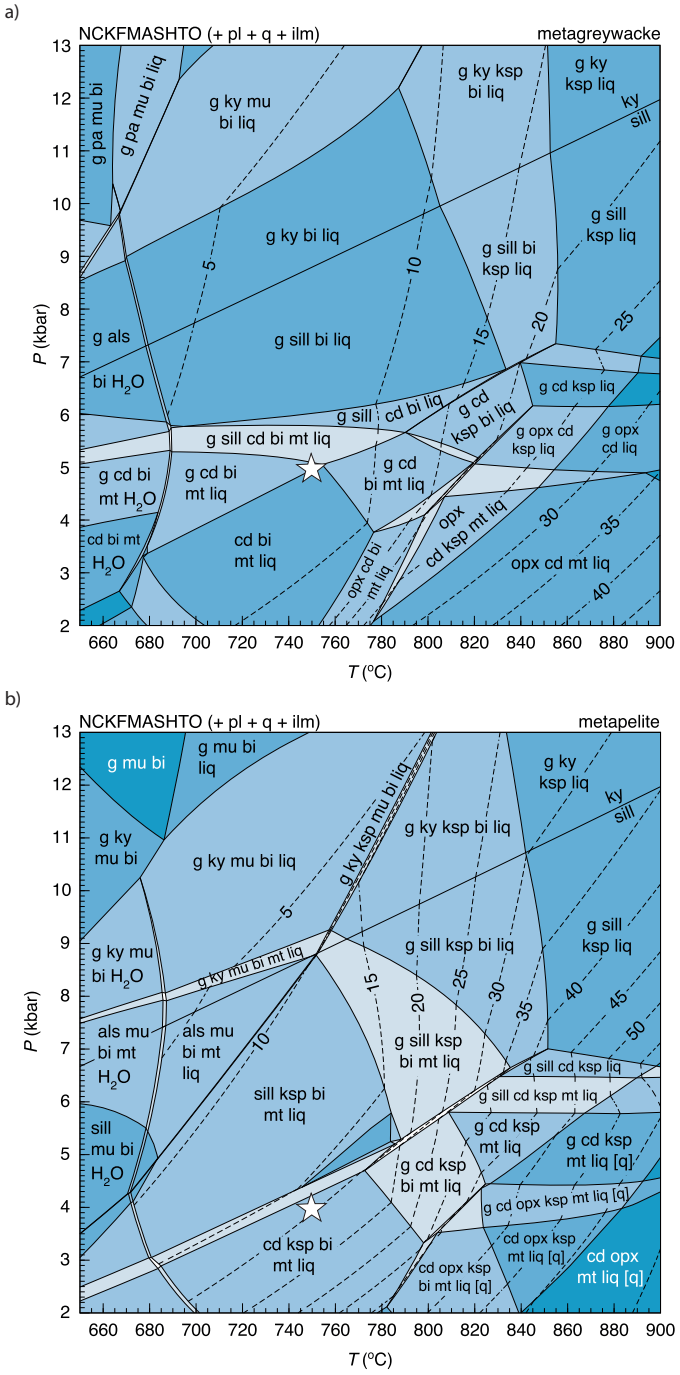

Figure 3.2: *P–T* pseudosections for the **(a)** metagreywacke composition of Yakymchuk & Brown (2014) and the **(b)** aluminous metapelite composition of Ague (1991). Dashed black lines indicate contours for the modal proportion of melt. White stars on all diagrams indicate the conditions of interest for partial melting, estimated by various authors including Ward *et al.* (2008) for aluminous metapelites. [Modified from Diener & Fagereng (2014, Fig. 3)]

dehydrates to K-feldspar and aluminosilicates at subsolidus conditions.

Diffusively-fluxed melting in aluminous metapelites is mostly identified in cordierite–biotite-bearing lithologies (Weinberg & Hasalová, 2015), such as the cordierite-bearing metapelites of the Kuiseb Schists in the Damara Belt described by (Ward *et al.*, 2008). The protolith composition of the Kuiseb Schist is comparable to the average metapelite composition of Ague (1991) and the P–T conditions are also representative of those where diffusively-fluxed melting has been described in other terranes (Weinberg & Hasalová, 2015). Therefore this case is selected to corroborate the modelling results. Whereas Ward *et al.* (2008) estimated melting to have occurred at conditions of 5 kbar and 750 °C, we conduct our modelling at a lower P of 4 kbar so that the observed presence of cordierite and absence of sillimanite is reproduced.

At these conditions, the aluminous metapelite which experiences muscovite melting is capable of producing a considerable volume of melt, up to $\sim$ 15 mol.%, through muscovite- and biotite–sillimanite melting (Fig. 3.2b). Examples of diffusively-fluxed melting in metapelites are estimated to have partially melted 10–40%, which is more than expected from fluid-absent melting alone. This discrepancy is further made evident with an aluminous metapelite that has undergone muscovite breakdown at subsolidus conditions. In this case, the metapelite would produce very little melt ($\sim$ 7 mol.%) at 750 °C and 4 kbar through biotite–sillimanite melting (Fig. 3.3a). Both cases are investigated and discussed further below.

3.2 Degree of fluid saturation and preconditioning of target lithologies

At the time when diffusively-fluxed melting starts, all the target lithologies would already have experienced a metamorphic history that will determine their H_2O content and degree of fluid saturation at the start of the process. For a normal prograde evolution, the target rocks are taken to have undergone subsolidus dehydration, such that they are fluid-saturated but contain minimal free H_2O at the wet solidus (Webb *et al.*, 2015). Therefore, the rocks have the maximum amount of hydrous minerals, but no excess H_2O (Table 3.2). This is the same starting condition that is typically inferred for modelling fluid-absent melting (e.g. White *et al.*, 2001; White, Powell, Holland, Johnson & Green, 2014; Yakymchuk & Brown, 2014; Webb *et al.*, 2015; Palin *et al.*, 2016; White *et al.*, 2017). This is the only condition considered for the tonalitic grey gneiss, TTG grey gneiss and metagreywacke compositions, because the very small amounts of melt produced by fluid-absent melting between the wet solidus and temperature conditions where diffusively-fluxed melting is modelled (750 °C) is unlikely to result in segregation and melt loss (White *et al.*, 2017; Yakymchuk & Brown, 2014). Therefore, these lithologies are not considered to undergo any melt loss, suprasolidus dehydration or preconditioning prior to diffusively-fluxed melting.

The metapelite, however, can experience either subsolidus muscovite breakdown (below

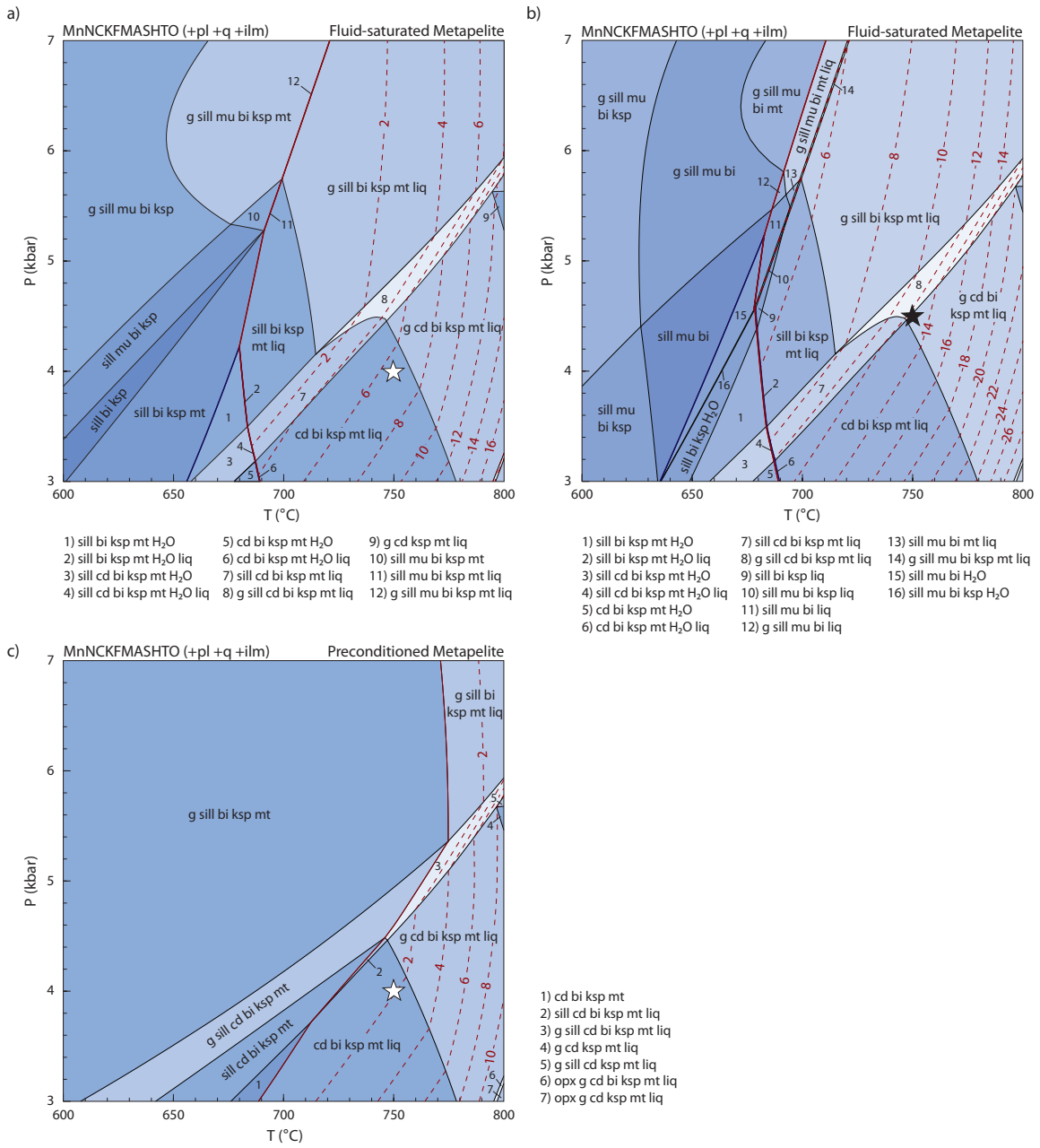

Figure 3.3: *P–T* pseudosections for the aluminous metapelite composition of Ague (1991) with variable H_2O content demonstrating **(a)** subsolidus muscovite breakdown, **(b)** muscovite dehydration melting at suprasolidus conditions and **(c)** the residuum or "preconditioned" composition after melt extraction at conditions marked by the black star on (b). Solid red and blue line indicate the solidus and H_2O saturation line, respectively. Dashed red lines indicate contours for the modal proportion of melt. White stars on all diagrams indicate the conditions of interest for partial melting.

4.5 kbar) or fluid-absent muscovite melting (above 4.5 kbar) prior to diffusively-fluxed melting. Therefore, both scenarios are considered: the first involves subsolidus muscovite breakdown (Fig. 3.3a) resulting in a fully-hydrated and fluid-saturated but muscovite-absent wet solidus assemblage (Table 3.2), whereas the second involves muscovite dehydration melting (Fig. 3.3b) and melt loss. The first scenario is the same as what we consider for the composite grey gneisses and metagreywacke composition. The second scenario results in a preconditioned metapelite composition, illustrated in Figure 3.3c, that has had 13 mol.% melt removed at 750 °C, leaving behind a fluid-undersaturated garnet-cordierite-bearing residuum containing less than 1% melt as the target lithology (Table 3.2).

3.3 Melt production, fluid sources and drivers of fluid flux

In all T-M_{H_2O} calculations, sufficient H_2O is added to each composition to produce more melt in a single event than what is inferred to have been cumulatively yielded by the examples documented in the literature. This is done to ensure that the modelling encompasses the entire interval over which melting could have occurred. For each lithology the H_2O content is varied from a minimum of 0 to a maximum of 12 mol.%, with the H_2O content of the initial condition for each lithology indicated by a white star on the T-M_{H_2O} pseudosections.

In order to investigate potential fluid sources and drivers of fluid flux, water-activity (a_{H_2O}) contours are calculated for each lithology and melting scenario, and these are translated to μ_{H_2O} values through the relationship

$$\mu_{H_2O} = \Delta G^0_{H_2O} + R\,T \ln a_{H_2O}, \tag{3.1}$$

where μ is chemical potential, ΔG^0 is the standard Gibbs energy of formation and R is the gas constant. These calculated μ_{H_2O} values are shown on the P–T–μ_{H_2O} diagrams presented for each lithology and fluid source.

The most likely candidate for a fluid source in the near- or suprasolidus mid- to lower continental crust is an ascending magma, with numerous case studies suggesting it as a fluid source (Collins *et al.*, 1989; Yardley & Barber, 1991; Holk & Taylor, 1997; Berger *et al.*, 2008). I-type magmas are the most probable source because of their abundance and fluid-rich nature (Wallace, 2005; Plank *et al.*, 2013). Upon ascent through the crust, these hydrous magmas can degas and exsolve H_2O that may lead to melting of the surrounding rocks (Plank *et al.*, 2013). Arc magmas are thus considered as a viable fluid source for diffusively-fluxed melting in the lower to mid-crust, with Collins *et al.* (2016) suggesting that this process is responsible for producing the voluminous Cordilleran batholiths.

For modelling the melting behaviour of the target rocks, we assume that there is an infinite supply of magma, such as can be approximated for migration along a conduit. This allows the fluid source to maintain a constant μ_{H_2O} even as fluid is fluxed to the target rocks, and

maximises the amount of melt that can be produced because melting is not limited by fluid availability. However, in the P–T–μ_{H_2O} calculations the actual H_2O content of the magma is considered because it determines the μ_{H_2O} of the fluid source, and therefore the direction of fluid flux. The H_2O content in arc magmas does not vary significantly, with a range of 2–6 wt.% H_2O and a common global average of 4 wt.% H_2O reported by Plank *et al.* (2013). Thus, we use these values in conjunction with the average I-type magma composition from Whalen *et al.* (1987, Table 3.1) to model the potential fluid source. We consider low-, typical- and high-H_2O content magmas as potential sources, having respectively 5 mol.% (∼1.5 wt.%), 13 mol.% (∼4 wt.%) and 20 mol.% (∼7 wt.%) H_2O. This brackets the natural range reported by Plank *et al.* (2013), while also accounting for somewhat extreme outliers.

Table 3.2: Bulk rock compositions (mol.%) used for phase diagram calculations

	Fig.	H_2O	SiO_2	Al_2O_3	CaO	MgO	FeO	K_2O	Na_2O	TiO_2	MnO	O	X_{Fe}
Ave. tonalitic	4.1a, c;	0.001	75.77	9.81	3.53	1.76	2.43	1.33	4.95	0.29	-	0.12	0.45
grey gneiss[a]	4.5a, b	12.00	66.68	8.63	3.11	1.55	2.14	1.17	4.36	0.25	-	0.11	0.45
Ave. TTG	4.1b, d;	0.001	77.46	9.95	2.94	0.93	1.54	1.84	4.98	0.21	-	0.15	0.43
grey gneiss[b]	4.5c	12.00	68.17	8.75	2.59	0.82	1.36	1.62	4.28	0.18	-	0.13	0.43
Ave.	4.2a, b;	0.001	77.79	8.21	1.16	3.57	4.20	1.27	2.85	0.52	0.10	0.32	0.15
metagreywacke[c]	4.5d	12.00	68.46	7.23	1.02	3.14	3.70	1.12	2.51	0.46	0.09	0.28	0.15
Fluid-sat.	4.3a, c;	0.001	61.68	13.04	1.52	5.28	7.68	2.81	1.91	0.87	0.17	1.27	0.33
metapelite[d]	4.6a	12.00	56.41	11.93	1.39	4.83	7.03	2.57	1.75	0.79	0.15	1.16	0.33
Preconditioned	4.3b, d;	0.001	62.04	14.05	1.69	6.08	8.84	2.76	1.88	1.00	0.19	1.46	0.33
metapelite[d]	4.6b	12.00	54.59	12.36	1.49	5.35	7.78	2.43	1.66	0.88	0.17	1.29	0.33
Ave. I-type	4.4, 4.5,	5.00	71.68	8.75	3.39	2.20	2.796	2.248	3.145	0.335	0.062	0.406	0.29
magma[e]	4.6	12.80	65.79	8.03	3.11	2.013	2.566	2.063	2.886	0.308	0.057	0.372	0.29
		20.00	60.36	7.37	2.86	1.847	2.354	1.893	2.648	0.282	0.052	0.342	0.29

Data sources are: [a]Moyen (2011); [b]Garde (1997); [c]Yakymchuk & Brown (2014); [d]Ague (1991); [e]Whalen *et al.* (1987).
X_{Fe} = FeO/(FeO+MgO)

Chapter 4

Modelling Results

4.1 Calculated mineral assemblages, melt volumes and a_{H_2O} contours

The mineral assemblage evolution and mineral and melt abundances during diffusively-fluxed melting are quantified through calculated T–M_{H_2O} pseudosections and associated modebox diagrams presented in Figures 4.1, 4.2 and 4.3. All diagrams are calculated at constant pressure of either 4, 5 or 6 kbar, as outlined above for the different lithologies. A temperature interval from subsolidus conditions of 625–650 °C to 800 or 820 °C is considered.

4.1.1 Tonalitic grey gneiss

The T–M_{H_2O} pseudosection for the average tonalitic grey gneiss composition of Moyen (2011) is shown in Figure 4.1a, with detailed mineral and melt proportions shown in a modebox calculated along an isothermal section at 750 °C in Figure 4.1c. This composition requires 1.2 mol.% H_2O to be just fluid-saturated at the wet solidus, and consists of plagioclase–quartz–biotite-bearing assemblages at most conditions. With excess H_2O at subsolidus conditions below 655 °C, it additionally contains minor amounts of augite, K-feldspar, titanite and hematite (Fig. 4.1a). For H_2O content below 1.2 mol.%, a subsolidus, H_2O-undersaturated orthopyroxene-bearing assemblage is stable over almost the entire temperature range considered (Fig. 4.1a). The composition is calculated to become melt-bearing for M_{H_2O} above 1.2 mol.% and temperatures above 655 °C. The co-existence of melt and H_2O is confined to the wet solidus, over a narrow field at 655 °C that extends from H_2O saturation at 1.2 mol.% to M_{H_2O} of 5.4 mol.%. K-feldspar is removed from the solidus assemblage at $M_{H_2O} = 5.4$ mol.%, allowing the wet solidus to gradually expand to higher temperature with increased M_{H_2O} (Fig. 4.1a).

The mineral assemblage changes at suprasolidus conditions are strongly dependent on temperature when K-feldspar is present, but become more dependent on M_{H_2O} and are deflected

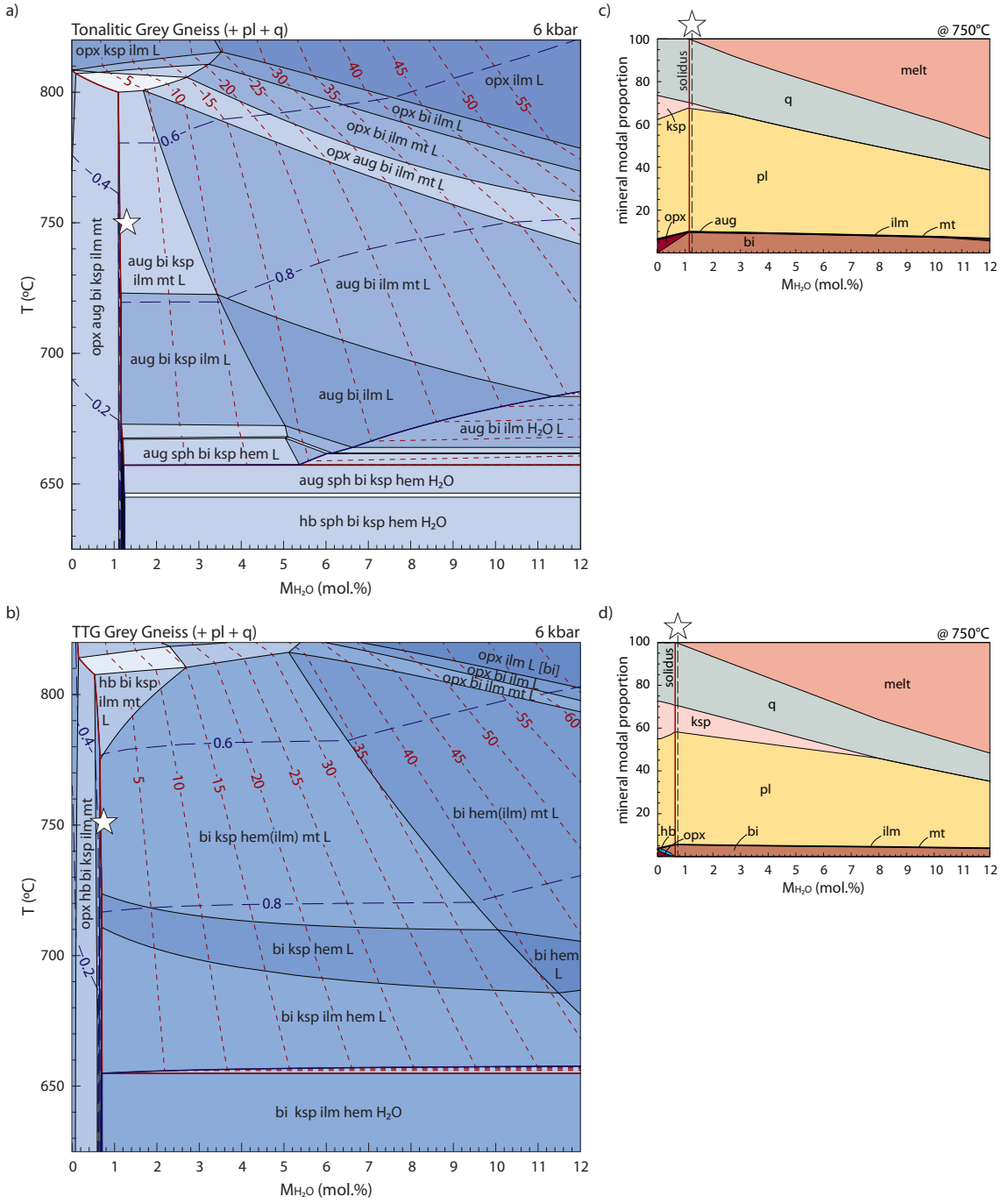

Figure 4.1: Calculated T–M_{H_2O} pseudosections and modebox plots for two average composite grey gneiss compositions. **(a)** T–M_{H_2O} pseudosection for the average tonalitic grey gneiss composition from Moyen (2011). **(b)** T–M_{H_2O} pseudosection for the average TTG grey gneiss composition from Garde (1997). Modebox plots **(c)** and **(d)** show the estimated mineral proportions calculated along an isothermal 750 °C section through (a) and (b), respectively. A bold red line indicates the solidus and H_2O saturation is shown by a bold blue line. The diagrams are contoured for melt abundance (red dashed lines) and for water-activity (blue dashed lines). The white stars on all diagrams indicate the conditions at which diffusively-fluxed melting initiates.

to lower temperature in the absence of K-feldspar (Fig. 4.1a). Conversely, the presence or absence of K-feldspar is primarily due to M_{H_2O} (Fig. 4.1a). In the presence of K-feldspar, magnetite is introduced at $\sim 720\,^{\circ}C$, followed by orthopyroxene at $800\,^{\circ}C$. Once orthopyroxene is present, augite, magnetite and biotite are removed in rapid succession towards higher temperature (Fig. 4.1a). The topology is the same in the absence of K-feldspar, but all the phase boundaries are gradually displaced to lower temperature with increasing M_{H_2O} (Fig. 4.1a). K-feldspar is only present in relatively dry compositions at suprasolius conditions, and its stability is restricted to lower M_{H_2O} with increased temperature. For example, K-feldspar coexists with melt between 1.2 and 4.2 mol.% H_2O at $700\,^{\circ}C$, but only between 1.2 and 2.6 mol.% H_2O at $750\,^{\circ}C$ (Fig. 4.1a). Biotite is the main hydrous mineral at suprasolidus conditions, and is only absent at temperatures above $780\,^{\circ}C$ towards higher M_{H_2O}. Melt production is strongly dependent on M_{H_2O} in relatively dry compositions ($M_{H_2O} < 5$ mol.%), but becomes more dependent on temperature once K-feldspar becomes absent at higher M_{H_2O} and/or orthopyroxene is introduced at higher temperature.

Progressive diffusively-fluxed melting at $750\,^{\circ}C$ will begin at the position of the white star and follow a horizontal line to higher M_{H_2O} on Fig. 4.1a-b, Fig. 4.2a and Fig. 4.3a-b. Figure 4.1c demonstrates the changes in mineral and melt abundance during the process. Prior to melting, at the conditions marked by the white star, the tonalitic grey gneiss composition is dominated by plagioclase ($\sim$ 57%) and quartz ($\sim$ 30%) with minor proportions of biotite ($\sim$ 10%) and K-feldspar ($\sim$ 2.5%; Fig. 4.1c). Augite, ilmenite and magnetite only occur in trace amounts. The sequence of melting can be described in intervals, each defined by the introduction or removal of a mineral. The first interval starts when diffusive flux begins and lasts until K-feldspar is exhausted. Within this interval, 1.4 mol.% H_2O is added to the initial fluid content to yield 7.2 mol.% melt, whereas 2.3 mol.% K-feldspar, plagioclase and quartz are consumed in equal proportions (Fig. 4.1c). The biotite content decreases slightly by 0.2 mol.%. The second interval occurs between the loss of K-feldspar and introduction of orthopyroxene, and involves the addition of a further 7.7 mol.% H_2O to produce 31.8 mol.% more melt. Plagioclase and quartz are the main reagents in this interval, decreasing by 19.6 mol.% and 9.9 mol.% respectively, whereas biotite abundance decreases slightly by 2.1 mol.%. The final melting interval occurs after the introduction of orthopyroxene, and spans a high M_{H_2O} range of 10.4–12 mol.%. In this interval, 1.5 mol.% biotite is consumed along with 3.7 mol% plagioclase and 2.8 mol.% quartz to produce a minor amount of melt (4.4 mol.%) and orthopyroxene (0.8 mol.%). Cumulatively, the tonalitic grey gneiss is calculated to produce more than 45 mol.% melt if it is diffusively fluxed with just less than 11 mol.% H_2O (Fig. 4.1c).

Calculated a_{H_2O} contours are primarily dependent on temperature at suprasolidus conditions, and decrease from unity at the wet solidus to $\sim$ 0.50 above $800\,^{\circ}C$ (Fig. 4.1a). The a_{H_2O} contours are exclusively dependent on temperature where K-feldspar is present, but are deflected to higher temperature with increasing H_2O content when K-feldspar is absent.

During melting at 750 °C, the tonalitic grey gneiss maintains an a_{H_2O} of $\sim$ 0.70 during the first melting interval, after which a_{H_2O} gradually increases to $\sim$ 0.80 when the composition contains 12 mol.% H_2O (Fig. 4.1a).

4.1.2 TTG grey gneiss

The T-M_{H_2O} pseudosection for the average TTG grey gneiss composition (Garde, 1997) is shown in Figure 4.1b, with detailed mineral and melt proportions shown in a modebox calculated along an isothermal section at 750 °C in Figure 4.1d. This composition requires 0.7 mol.% H_2O to be fluid-saturated at the wet solidus, and consists of plagioclase–quartz–biotite-bearing assemblages at most conditions. With excess H_2O at subsolidus conditions below 655 °C, this composition additionally contains K-feldspar and minor ilmenite and hematite (Fig. 4.1b). For H_2O content below 0.7 mol.%, the TTG gneiss composition is calculated to contain a subsolidus, H_2O-undersaturated orthopyroxene-bearing assemblage over the entire temperature range considered. The coexistence of melt and H_2O is confined to a narrow field at the wet solidus at $\sim$ 655 °C across the entire range of M_{H_2O} considered (Fig. 4.1b).

The only significant mineral assemblage changes that occur at suprasolidus conditions are the introduction of orthopyroxene at more than 800 °C, which is coupled to the removal of magnetite and biotite, and the exhaustion of K-feldspar at high temperatures and M_{H_2O} (Fig. 4.1b). Hornblende is present at near-solidus M_{H_2O} values at temperatures above 775 °C. K-feldspar persists to higher M_{H_2O} in the TTG grey gneiss than the tonalite composition, and is only removed once $\sim$ 10 mol.% H_2O is added at 700 °C, or when $\sim$ 7.3 mol.% H_2O is added at 750 °C. Biotite is the main hydrous mineral at suprasolidus conditions and is only removed once orthopyroxene is introduced above 800 °C. Similar to the tonalite composition, the melt contours are largely dependent on M_{H_2O} in relatively dry compositions ($M_{H_2O}<$ 5 mol.%), but become more dependent on temperature at higher M_{H_2O} and temperatures (Fig. 4.1b).

Progressive diffusively-fluxed melting at 750 °C is calculated to initiate in a TTG grey gneiss protolith composition dominated by plagioclase ($\sim$ 52%) and quartz ($\sim$ 29%) with minor proportions of biotite ($\sim$ 5%), K-feldspar ($\sim$ 12%) and trace amounts of oxides (Fig. 4.1d). The initial melting interval continues until K-feldspar is exhausted and involves the addition of 7.2 mol.% H_2O to yield 35.5 mol.% melt. 12.3 mol.% K-feldspar, 11.1 mol.% quartz, 11 mol.% plagioclase and a minor amount of biotite (1.1 mol.%) are consumed over this interval (Fig. 4.1d). The second melting interval encompasses the removal of K-feldspar to the maximum H_2O content considered, and involves the addition of a further 4.1 mol.% H_2O to increase the melt abundance by 15.9 mol.%. Plagioclase is the main reagent, decreasing by 10.1 mol.%, whereas 5 mol.% quartz is also consumed along with a minor amount of biotite (0.7 mol.%). Cumulatively, this TTG grey gneiss composition is marginally more fertile than the tonalitic grey gneiss, yielding 52 mol.% from diffusive fluxing of a bit more than 11 mol.%

H_2O (Fig. 4.1d).

Calculated a_{H_2O} contours are largely dependent on temperature at suprasolius conditions, decreasing gradually from unity at the wet solidus to 0.50 above 800 °C (Fig. 4.1b). Where K-feldspar is present, a_{H_2O} contours are exclusively dependent on temperature, but are displaced to higher temperature with increasing M_{H_2O} when K-feldspar is absent. Progressive melting at 750 °C of the TTG grey gneiss occurs at a sustained a_{H_2O} of $\sim$ 0.70 until K-feldspar is consumed, after which a_{H_2O} gradually increases to $\sim$ 0.75 when the composition contains 12 mol.% H_2O (Fig. 4.1b).

4.1.3 Metagreywacke

The calculated T–M_{H_2O} pseudosection for the average metagreywacke composition is shown in Figure 4.2a with detailed melt and mineral proportions calculated at 5 kbar along an isothermal section at 750 °C presented in Figure 4.2b. This composition requires 2.2 mol.% H_2O to be fluid-saturated at the wet solidus, and contains a garnet–sillimanite–cordierite–biotite–plagioclase–quartz–ilmenite assemblage at H_2O-saturated subsolidus conditions. At fluid-undersaturated subsolidus conditions ($M_{H_2O} < 2$ mol.%), garnet and K-feldspar are present over the entire range of temperatures considered, and occur in conjunction with sillimanite at lower T or cordierite at higher T (Fig. 4.2a). Melt and free H_2O only co-exist over a narrow field at the wet solidus at 697–700 °C for M_{H_2O} between 2.2 and 8.4 mol.%. At M_{H_2O} higher than 8.4 mol.%, melt–H_2O coexistence begins to extend to somewhat higher temperatures, up to 710 °C at 12 mol.% H_2O.

The main mineral assemblage changes at suprasolidus conditions are the introduction of K-feldspar in relatively dry compositions ($M_{H_2O} < 3$ mol.%) at 760 °C, which is coupled to the removal of sillimanite (Fig. 4.2a). In the absence of K-feldspar, sillimanite is lost at progressively lower temperatures with increasing M_{H_2O}. Orthopyroxene is only introduced at the highest M_{H_2O} at temperatures approaching 800 °C, following which biotite is removed. As with the composite grey gneiss compositions, biotite is the main hydrous mineral at suprasolidus conditions, and remains stable until orthopyroxene is introduced (Fig. 4.2a). The shape of melt contours for the metagreywacke are also similar to those of the grey gneisses, being primarily dependent on M_{H_2O} in relatively dry compositions ($M_{H_2O}< 5$ mol.%), but becoming more dependent on temperature at higher M_{H_2O} and temperatures (Fig. 4.2a).

Progressive diffusively-fluxed melting of the metagreywacke at 750 °C initiates in an assemblage consisting mostly of quartz ($\sim$ 44%) and plagioclase ($\sim$ 30%) with minor proportions of biotite ($\sim$ 14%), cordierite ($\sim$ 7%), sillimanite ($\sim$ 2%) and garnet ($\sim$ 2%; Fig. 4.2b). Ilmenite and magnetite only occur in trace amounts, and this assemblage is notably devoid of K-feldspar. The first melting interval continues until sillimanite is exhausted, and involves the addition of 1.6 mol.% H_2O to the solidus fluid content of 2.2 mol.% H_2O. This interval yields 8.2 mol.% melt in conjunction with the production of 3.1 mol.% cordierite and 0.2 mol.% garnet at the expense of 1.7 mol.% sillimanite, 2.7 mol.% biotite, 3.2 mol.% pla-

gioclase and 4 mol.% quartz (Fig. 4.2b). Once sillimanite is exhausted, the influx of a further 8.2 mol.% H_2O yields 35.6 mol.% melt and 2.8 mol.% garnet, whereas 16.8 mol.% plagioclase, 13.9 mol.% quartz, 5.5 mol.% biotite and 2.3 mol.% cordierite are consumed. Cumulatively, the metagreywacke is calculated to produce a total of 45 mol.% melt from diffusive fluxing of just less than 10 mol.% H_2O.

As with the grey gneiss compositions, calculated a_{H_2O} contours for the metagreywacke at suprasolidus conditions show a strong dependence on temperature, and decrease from unity at the wet solidus to ~ 0.60 at 800 °C (Fig. 4.2a). The contours are exclusively dependent on temperature where K-feldspar or sillimanite are present, but are deflected towards higher temperature with increasing H_2O content in their absence. Progressive melting at 750 °C occurs at a sustained a_{H_2O} of ~ 0.75 during the first interval while sillimanite is being consumed, before increasing gradually to ~ 0.90 during the subsequent, sillimanite-absent melting interval.

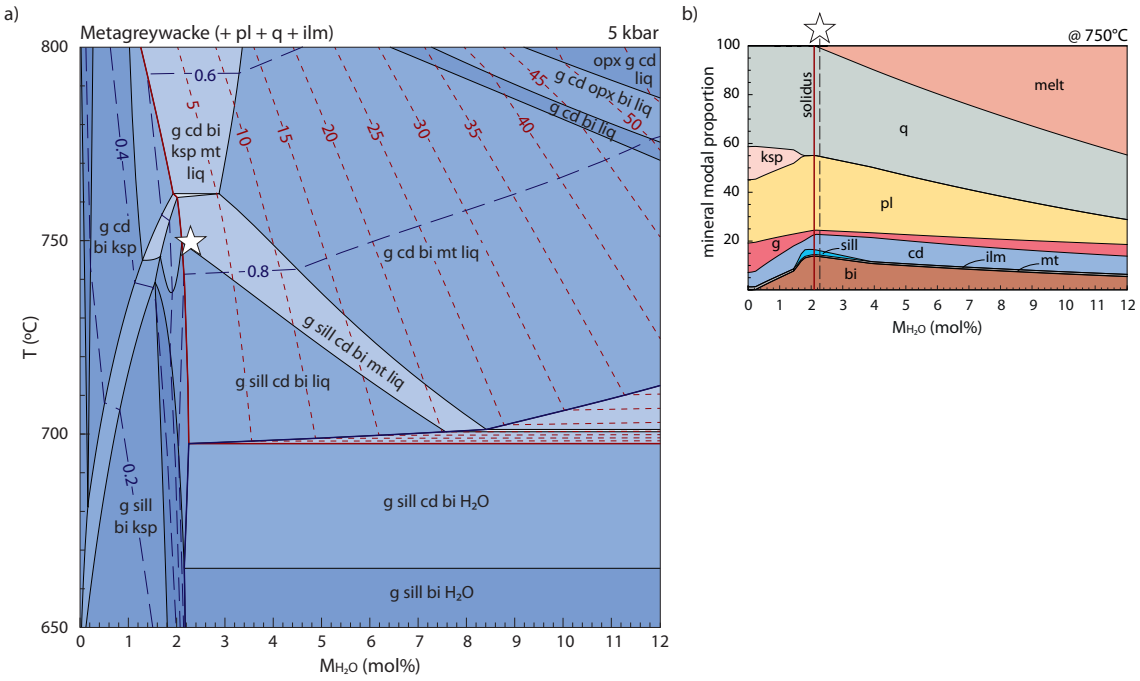

Figure 4.2: Calculated T–M_{H_2O} pseudosection for **(a)** the average metagreywacke composition from Yakymchuk & Brown (2014). **(b)** Modebox plot showing the predicted mineral proportions along an isothermal 750 °C section through (a). A bold red line indicates the solidus, with a bold blue line showing H_2O saturation. The diagram is contoured for melt abundance (red dashed lines) and for water-activity (blue dashed lines). The white star indicates the conditions at which diffusively-fluxed melting initiates.

4.1.4 Fluid-saturated aluminous metapelite

The T–M_{H_2O} pseudosection for the aluminous metapelite composition is shown in Figure 4.3a, and calculated melt and mineral abundances along an isothermal section at 750 °C and 4

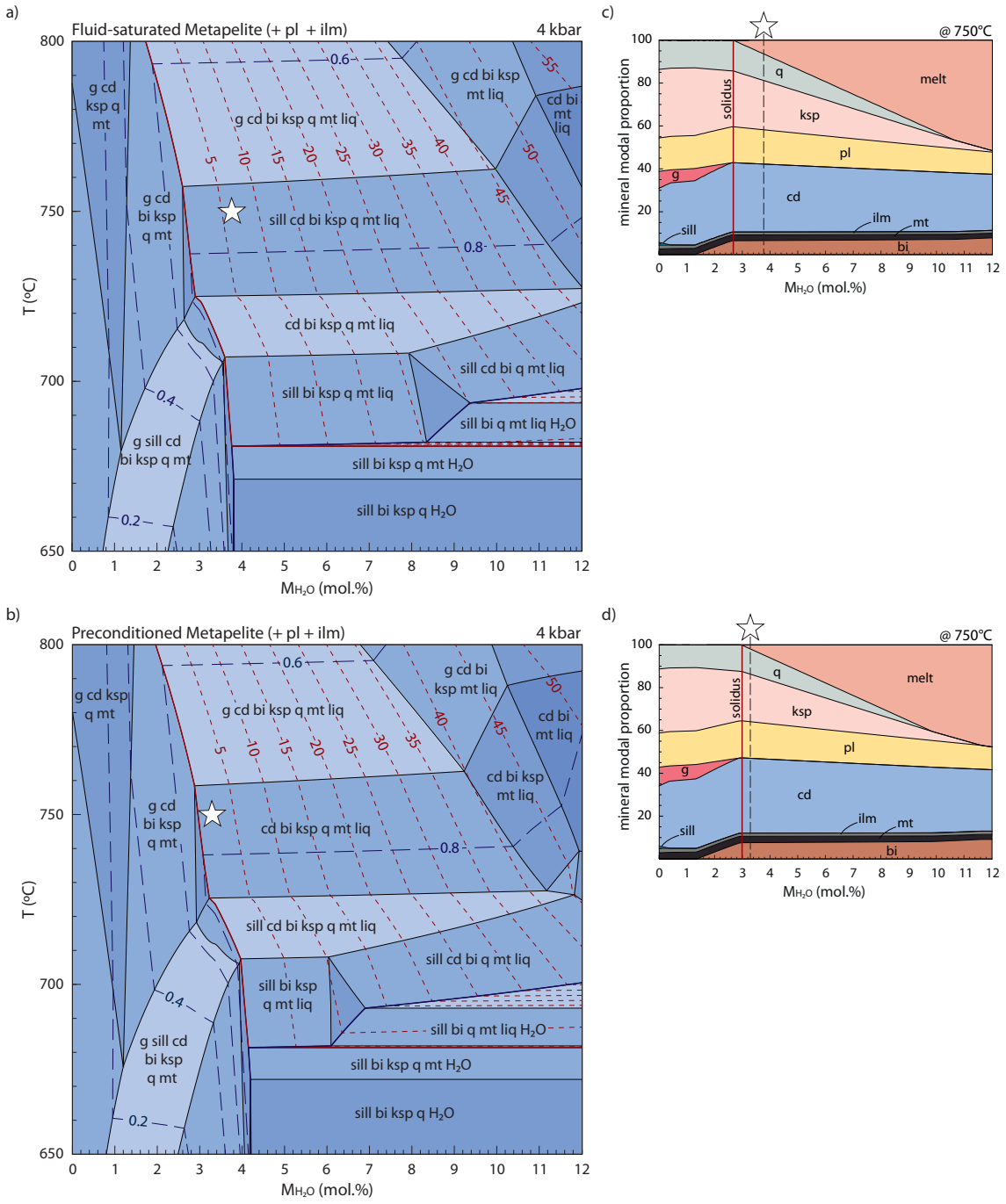

Figure 4.3: Calculated T–M_{H_2O} pseudosections and modebox plots for the average aluminous metapelite composition from Ague (1991). **(a)** T–M_{H_2O} pseudosection for the fluid-saturated aluminous metapelite composition, which has experienced subsolidus muscovite breakdown. **(b)** T–M_{H_2O} pseudosection for the preconditioned aluminous metapelite composition, which experienced suprasolidus muscovite dehydration melting before melt loss. Modebox plots **(c)** and **(d)** show the estimated mineral proportions along an isothermal 750 °C section through (a) and (b), respectively. A bold red line indicates the solidus and H_2O saturation is shown by a bold blue line. The diagrams are contoured for melt abundance (red dashed lines) and for water-activity (blue dashed lines). The white stars on all diagrams indicate the conditions at which diffusively-fluxed melting initiates.

kbar in Figure 4.3c. This composition requires 3.8 mol.% H_2O to be H_2O-saturated at the wet solidus, and contains a sillimanite–biotite–K-feldspar–plagioclase–quartz–ilmenite–magnetite assemblage at H_2O-saturated subsolidus conditions (Fig. 4.3a). Assemblages of garnet–cordierite–K-feldspar–plagioclase–ilmenite–magnetite ± biotite ± sillimanite occur at H_2O-undersaturated subsolidus conditions in compositions with M_{H_2O} below 2–3.8 mol.% H_2O (Fig. 4.3a). The coexistence of melt and free H_2O only occurs at the wet solidus at 680 °C for M_{H_2O} between 3.8 and 8.4 mol.%. K-feldspar is absent at higher M_{H_2O}, allowing H_2O–melt coexistence to gradually expand to higher temperatures, up to 700 °C at 12 mol.% H_2O.

The fluid-saturated metapelite composition experiences a number of suprasolidus mineralogical changes that are almost exclusively dependent on temperature when K-feldspar and quartz are present (Fig. 4.3a). Cordierite is introduced at 705 °C, before sillimanite is removed at 725 °C, following which garnet is introduced at 760 °C (Fig. 4.3a). In the absence of K-feldspar or quartz, these phase boundaries become more dependent on M_{H_2O} and are deflected to lower temperature in the absence of K-feldspar, or higher temperature in the absence of quartz. The stability of K-feldspar and quartz have a strong dependence on M_{H_2O} (Fig. 4.3a). For temperatures below 725 °C, K-feldspar is the only phase to be exhausted with increasing M_{H_2O}, whereas at higher T, quartz is lost before K-feldspar. Between ∼680 and 725 °C, the addition of at least 4 mol.% H_2O to the initial fluid content of 3.8 mol.% is required to remove K-feldspar. Conversely, the loss of quartz above 725 °C requires the addition of at least 4–8 mol.% H_2O, with less H_2O required at higher temperature (Fig. 4.3a). The shape of calculated melt contours mimics that of the dry solidus and increase primarily with M_{H_2O} until ∼ 20 mol.% melt, after which it becomes more dependent on temperature (Fig. 4.3a).

Prior to the initiation of diffusively-fluxed melting at 750 °C, the fluid-saturated metapelite will already have produced ∼ 7 mol.% melt through the dehydration melting of sillimanite + biotite (e.g. Spear *et al.*, 1999; White *et al.*, 2001). As outlined, this melt is assumed to be retained here, to contrast it to the melt-depleted and preconditioned metapelite example below. Therefore diffusively-fluxed melting starts in a composition consisting of cordierite (∼ 32%), K-feldspar (∼ 23%), plagioclase (∼ 16%) quartz (∼ 12%), biotite (∼ 7%), melt (∼ 7%) and minor magnetite and ilmenite (white star in Figs. 4.3a and 4.3c). As diffusively-fluxed melting proceeds, quartz is the first phase to be exhausted after the addition of 6.8 mol.% H_2O to the initial fluid content, with 40.1 mol.% melt and 0.6 mol.% biotite being produced at the expense of 19 mol.% K-feldspar, 12.3 mol.% quartz, 4.7 mol.% plagioclase and 4.2 mol.% cordierite. The next melting interval continues in the absence of quartz until the maximum M_{H_2O}, encompassing the addition of a further 1.4 mol.% H_2O to yield 4.9 mol.% melt and 0.7 mol.% biotite while consuming 3.2 mol.% K-feldspar, 1 mol.% plagioclase and 1.3 mol.% cordierite (Fig. 4.3c). Diffusively-fluxed melting of the fluid-saturated metapelite at 750 °C produces ∼ 45 mol.% melt for the addition of 8.2 mol.% H_2O.

As with other compositions, calculated a_{H_2O} contours are temperature-dependent at suprasolidus conditions in the presence of quartz and K-feldspar, and decrease from unity at the wet solidus to ~ 0.60 at 800 °C (Fig. 4.3a). The a_{H_2O} contours are displaced towards higher temperature with increasing H_2O once either of these phases is exhausted. Progressive melting of the fluid-saturated metapelite at 750 °C is calculated to largely proceed at a constant a_{H_2O} of ~ 0.75, only increasing to ~ 0.80 once quartz is depleted at extreme M_{H_2O} values.

4.1.5 Preconditioned aluminous metapelite

The T–M_{H_2O} pseudosection for the preconditioned aluminous metapelite composition is shown in Figure 4.3b. Mineral and melt proportions are indicated in the modebox calculated at 4 kbar along an isothermal section at 750 °C in Figure 4.3d. After melt extraction, this composition has an H_2O content of 3.3 mol.% which is maintained until the initiation of diffusively-fluxed melting. The topology, position of phase boundaries and shape of melt contours on the pseudosection for the preconditioned metapelite are exactly the same as that of the fluid-saturated metapelite composition, with the notable difference that K-feldspar and quartz are both removed at significantly lower values of M_{H_2O} (Fig. 4.3b).

Diffusively-fluxed melting at 750 °C starts in an initial composition that consists of cordierite ($\sim$ 35%), K-feldspar ($\sim$ 22%), plagioclase ($\sim$ 17%), quartz ($\sim$ 12%), biotite ($\sim$ 8%) and trace amounts of ilmenite, magnetite and melt (white star in Figs 4.3b and 4.3d). As melting progresses with increasing M_{H_2O}, quartz is the first phase to be consumed once 6.6 mol.% H_2O is added to the initial fluid content. This first melting interval produces 37.5 mol.% melt and 0.5 mol.% biotite at the expense of 18.1 mol.% K-feldspar, 11.8 mol.% quartz, 4.7 mol.% plagioclase and 4.3 mol.% cordierite. After the loss of quartz, K-feldspar is depleted once a further 1.7 mol.% H_2O is added. In this interval, 6.4 mol.% melt and 1 mol.% biotite are produced whereas 4.2 mol.% K-feldspar, 1.2 mol.% plagioclase and 1.7 mol.% cordierite are consumed (Fig. 4.3d). The final melting interval occurs in the absence of both K-feldspar and quartz, and involves the influx of 0.4 mol.% H_2O to yield an additional 0.8 mol.% melt at the expense of 0.3 mol.% cordierite and 0.5 mol.% plagioclase (Fig. 4.3d). Cumulatively, the preconditioned metapelite produces 45 mol.% melt from the addition of 8.7 mol.% H_2O.

Calculated a_{H_2O} contours at suprasolidus conditions are largely dependent on temperature and decrease from unity at the wet solidus to ~ 0.60 at 800 °C (Fig. 4.3b). In the presence of K-feldspar and/or quartz, a_{H_2O} is entirely dependent on temperature. Once these phases are exhausted, the a_{H_2O} contours are steeply diverted to higher temperature with increasing M_{H_2O}. Diffusively-fluxed melting of the preconditioned metapelite proceeds at a constant $a_{H_2O} \sim 0.75$ until quartz is exhausted. Thereafter, it increases to ~ 0.82 by $M_{H_2O} = 12$ mol.%.

4.1.6 Summary

Despite their compositional differences, all the target lithologies show the same trends with the influx of external fluids. In all cases, the T conditions that allow for the coexistence of

water and melt as two separate phases is extremely limited, and confined to wet solidus temperatures, particularly where K-feldspar—or sillimanite in the case of the metagreywacke—are present. In the absence of these minerals the stability of coexisting melt and water expands to somewhat higher temperatures with increasing water content, but never extends above 700–710 °C (Figs. 4.1a, b, 4.2a, 4.3a, b). The overall melt fertility and the rate of melt production is also similar for all lithologies, with ∼ 5–6 mol.% melt yielded for each mol.% of H_2O added, such that all lithologies are modelled to produce 45–50 mol.% for the H_2O range considered (Figs. 4.1c, d, 4.2b, 4.3c, d). Melting also preferentially consumes K-feldspar, quartz and plagioclase in all samples. Notably, biotite, as the principal hydrous mineral in all samples, mostly maintains its relative abundance and only undergoes small increases or decreases in abundance during progressive melting, indicating that it does not readily participate in the melting process.

a_{H_2O} also shows similar behaviour in all examples (Figs. 4.1a, b, 4.2a, 4.3a, b). In the presence of K-feldspar and quartz, a_{H_2O} is exclusively a function of temperature such that constant a_{H_2O} of 0.70 for the composite grey gneisses and 0.75 for the metagreywacke and metapelite targets are maintained even as moderate to large volumes of H_2O are fluxed during progressive melting. However, once K-feldspar or quartz is consumed, the a_{H_2O} of the target lithology gradually increases to around 0.80. The effects of this are investigated in the next section.

4.2 P–T–μ_{H_2O} relations and directions of fluid flux

In order for the melting process described above to proceed, H_2O must be able to flux from the fluid source into the target rocks. On a large scale, the fluid source first has to come into proximity with the target rocks, through a mechanism such as physical migration of a magma, but locally the movement of H_2O from the source into the target rocks is a diffusive process driven by the chemical potential gradient of H_2O (μ_{H_2O}), and requires the chemical potential of the source to be higher than that of the target rocks (cf. White & Powell, 2010). H_2O will continue to diffuse until μ_{H_2O} of the source and target are the same, and no μ_{H_2O} gradient exists any more. For the purpose of this study, 'forward flux' describes a scenario where H_2O diffuses from the fluid source with a higher μ_{H_2O} to the target lithology with a lower μ_{H_2O}. Alternatively, if H_2O diffuses from the target rock to the fluid source, this scenario is described as 'reverse flux'.

Figure 4.4 presents the phase relations for the proposed I-type magma fluid source encompassing the low, typical and high H_2O content range reported by Plank *et al.* (2013), calculated over a T range of 650–800 °C at 6 kbar. The melt content of the I-type magma depends on both its H_2O content and temperature (Fig. 4.4). For the inferred temperature of diffusively-fluxed melting at 750 °C, the low-H_2O source only contains 20 mol.% melt, close to the minimum necessary for the magma to behave as a liquid (Arzi, 1978; van der Molen & Pa-

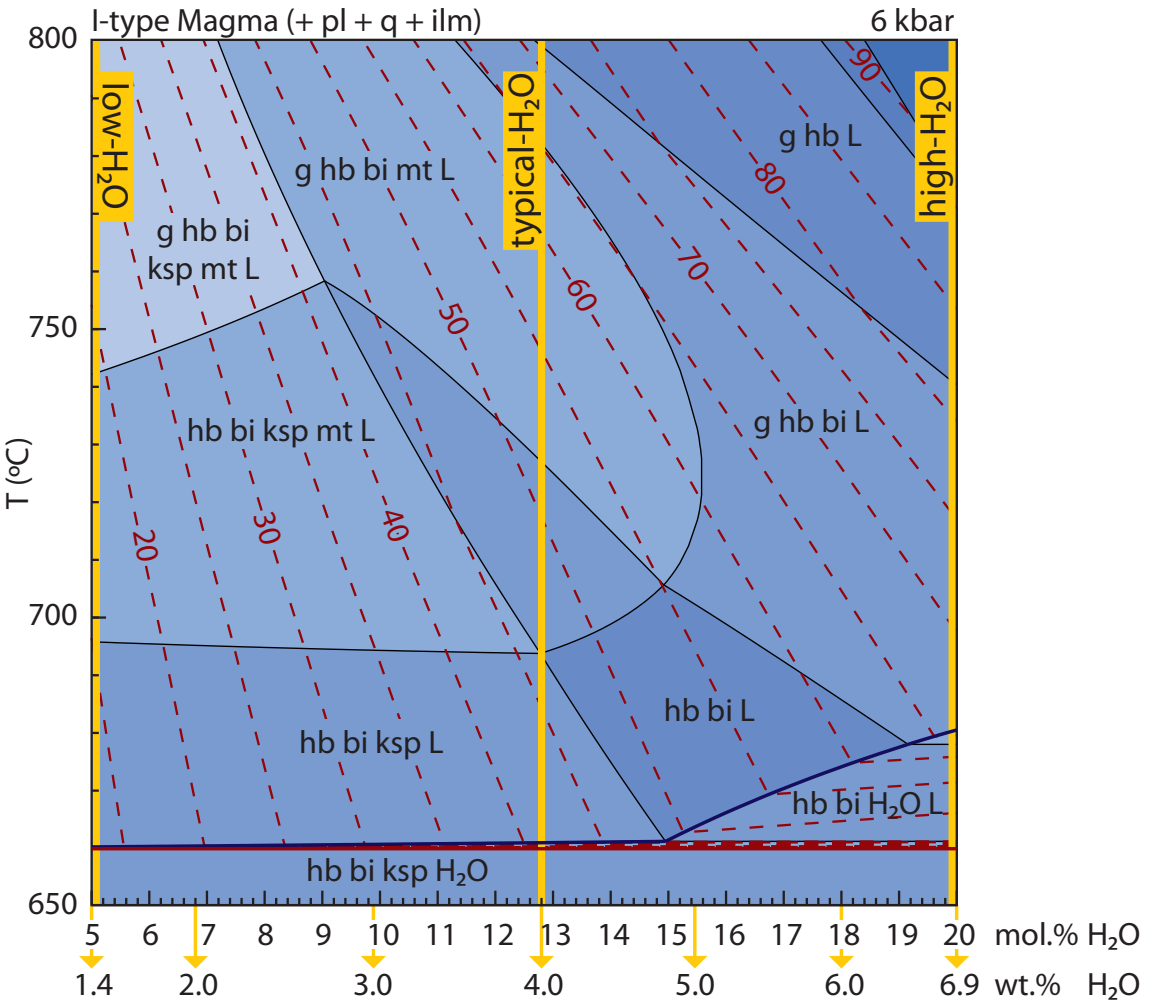

Figure 4.4: Calculated T-M_{H_2O} pseudosection at 6 kbar for the average I-type magma of Whalen *et al.* (1987). The bold red line indicates the solidus and H_2O saturation is shown by a bold blue line. Melt abundance contours are shown as red dashed lines and the three magma compositions discussed in the text are marked by thick yellow lines.

terson, 1979; Rosenberg & Handy, 2005). The magma with typical-H_2O contains more than 55 mol.% melt, whereas the high-H_2O magma contains almost 85 mol.% melt (Fig. 4.4).

The calculated P–T–μ_{H_2O} relations of the different target lithologies and idealised I-type magma fluid sources are presented in Figures 4.5 and 4.6. Unlike Figures 4.1–4.4, these diagrams are calculated as a function of pressure to simulate the ascending magma fluid source and to investigate whether there is a limitation on the crustal depth at which diffusively-fluxed melting can occur. Figure 4.5a presents a general overview of how the process works, using the tonalitic grey gneiss target and I-type magma with typical H_2O content as an example, and considering a range of mid-crustal pressures from 4 to 8 kbar, and variable temperatures of 700, 730 and 750 °C. Following this, the detailed behaviour of the different target lithologies and I-type magma source with variable H_2O content are calculated at 750 °C and presented in Figure 4.5b–f.

4.2.1 Tonalitic grey gneiss

Prior to melting, the tonalitic grey gneiss target has a lower μ_{H_2O} than the I-type magma at all P–T conditions considered (Fig. 4.5a). This means that H_2O will be able to diffusively flux from the magma to the target rocks and drive the melting process (i.e. forward flux). Because the I-type magma is assumed to have an infinite volume, removal of H_2O does not affect the μ_{H_2O} of the source. However, melting of the tonalitic grey gneiss composition gradually increases its μ_{H_2O}. After 15 mol.% melt has been produced at 750 °C, the μ_{H_2O} value of the target and source can be seen to cross over at 7.3 kbar (Fig. 4.5a). For pressure below 7.3 kbar, μ_{H_2O} of the target is lower than that of the source, and forward flux and further melting will occur, but for pressure above 7.3 kbar, melting will cease as reverse flux will occur and H_2O will diffuse from the target back into the source. Once 30 mol.% melt has been produced, only target rocks at pressures below 4.2 kbar will still be capable of forward flux and additional melting (Fig. 4.5a). The same situation occurs for melting at 730 °C, but with the crossover at 6.9 kbar once 15 mol.% melt has been produced. The target will furthermore yield less than 30 mol.% melt over the entire pressure range before μ_{H_2O} are equalised (Fig. 4.5a). At 700 °C, the target will still experience forward flux and additional melting over the entire pressure range once 15 mol.% melt has been produced, but melting will cease shortly after and μ_{H_2O} will be equalised before 30 mol.% melt is produced (Fig. 4.5a).

Figure 4.5b illustrates the μ_{H_2O} behaviour of the average tonalitic grey gneiss with average I-type magmas of variable H_2O content, at 6 kbar and 750 °C. Prior to melting, the target tonalitic grey gneiss composition consistently has a μ_{H_2O} lower than all three H_2O sources, implying that forward flux will occur and melting will commence regardless of the source's H_2O content. With increasing amounts of melt, the μ_{H_2O} of the target composition does not increase in a regular manner. Whereas there is a negligible change in μ_{H_2O} for the first 5 mol.% of melting, μ_{H_2O} then increases rapidly up to 15 mol.% melt, after which it increases

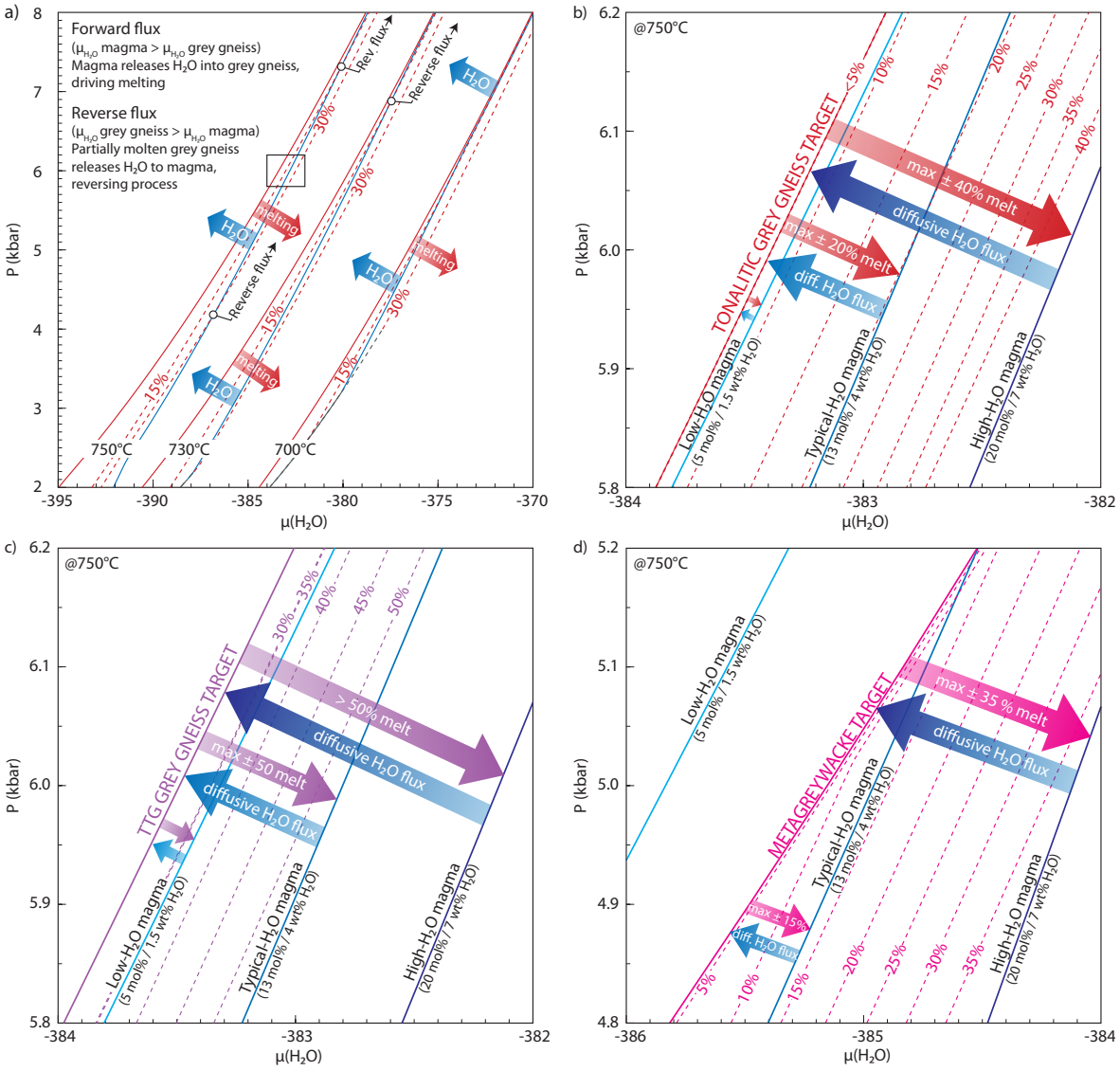

Figure 4.5: Calculated P–T–μ_{H_2O} diagrams. **(a)** Calculated μ_{H_2O} of the average I-type magma with typical H_2O content at 700, 730 and 750 °C (blue solid lines) compared to μ_{H_2O} of the tonalitic grey gneiss protolith (red solid lines). Red dashed lines show calculated μ_{H_2O} of the tonalitic grey gneiss after different degrees of melting as shown. Box at 6 kbar indicates the part of the diagram enlarged in (b). **(b–d)** μ_{H_2O} relations calculated at 750 °C for (b) the tonalitic grey gneiss composition, (c) TTG grey gneiss composition and (d) metagreywacke composition relative to that of an I-type magma with low, typical and high H_2O content. Large solid arrows are schematic, indicating the direction of diffusive H_2O flux and coupled shift in μ_{H_2O} of the target lithology with progressive melting.

more gradually with further melting (Fig. 4.5b).

Consequently, the μ_{H_2O} gradient between the low-H_2O magma and the target tonalitic grey gneiss is sustained until the target consists of ∼10 mol.% melt, after which μ_{H_2O} are equalised. For a source magma with typical H_2O content, 20 mol.% melt is produced before the process is terminated. The high-H_2O magma composition has a very high μ_{H_2O} relative to the target composition, such that more than 45 mol.% melt is produced before μ_{H_2O} are equalised (Fig. 4.5b).

4.2.2 TTG grey gneiss

Figure 4.5c shows that the interaction of the TTG grey gneiss composition and I-type magma fluid sources are similar to that of the tonalitic grey gneiss at 6 kbar and 750 °C. The TTG grey gneiss composition has a lower μ_{H_2O} than all three fluid sources prior to melting, such that melting will initiate regardless of the source magma's H_2O content. As the amount of melt increases, the calculated μ_{H_2O} of the target composition increase in an irregular manner. For the first 35 mol.% of melting, the overall change in μ_{H_2O} is minor; however, further melting rapidly increases the μ_{H_2O} of the system (Fig. 4.5c). Consequently, a low-H_2O magma is calculated to yield enough H_2O for $\sim$ 35 mol.% melting of the TTG grey gneiss before μ_{H_2O} are equalised. Similarly, a typical I-type magma is capable of inducing $\sim$ 50% melting in the target composition whereas a high-H_2O magma can induce the production of more than 50 mol.% melt (Fig. 4.5c).

4.2.3 Metagreywacke

The calculated behaviour of the average metagreywacke composition and the various I-type magma fluid sources at 5 kbar and 750 °C is shown in Figure 4.5d. A notable difference compared to the grey gneiss compositions is that a low-H_2O magma has a lower μ_{H_2O} than the metagreywacke, such that it is not capable of inducing any melting. This implies that for forward fluxing to occur and melting to ensue, the magma fluid source must be sufficiently rich in H_2O (>13 mol.% / 4 wt.% H_2O). A further distinction is that μ_{H_2O} of the metagreywacke is strongly dependent on pressure, such that a typical magma fluid source will only induce melting below 5.2 kbar (Fig. 4.5d). Like the other lithologies, calculated μ_{H_2O} of the metagreywacke composition does not increase in a regular manner as melting proceeds. There is only a minor change in μ_{H_2O} for the first 10% of melting, following which μ_{H_2O} increases rapidly up to 20 mol.% melt, after which it again increases more gradually (Fig. 4.5d). For pressures where melting of the metagreywacke is feasible (< 5 kbar), the I-type magma with typical H_2O content is calculated to induce less than $\sim$ 15% melting before μ_{H_2O} are equalised. A magma with high H_2O content can induce the production of $\sim$ 35 mol.% melt from the metagreywacke composition (Fig. 4.5d).

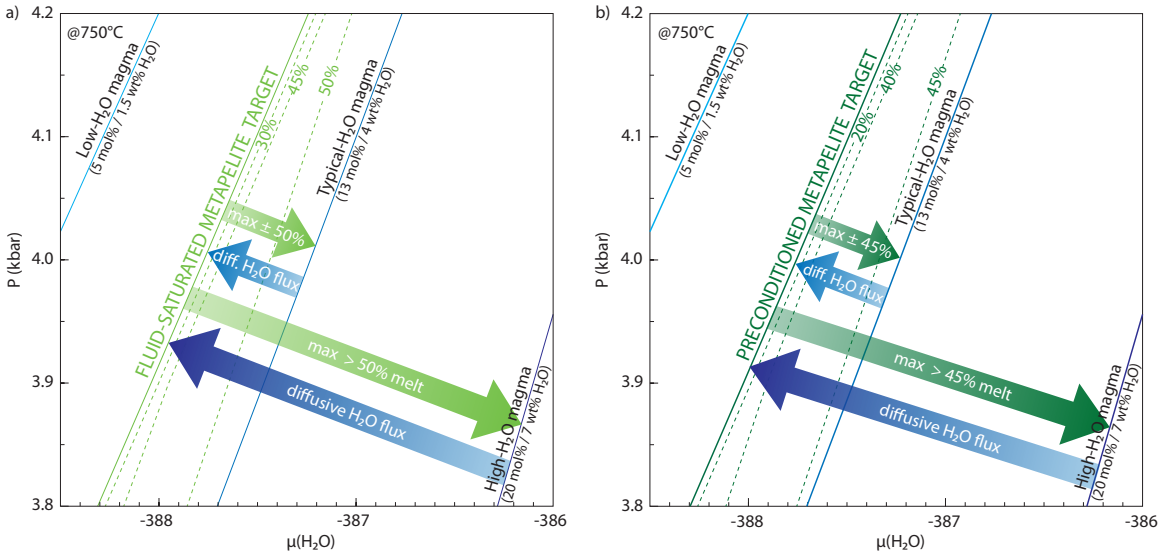

Figure 4.6: Calculated P–T–μ_{H_2O} diagrams. **(a & b)** μ_{H_2O} relations calculated at 750 °C for the (a) fluid-saturated aluminous metapelite and (b) preconditioned aluminous metapelite composition relative to that of an I-type magma with low, typical and high H_2O content. Large solid arrows are schematic, indicating the direction of diffusive H_2O flux and coupled shift in μ_{H_2O} of the target lithology with progressive melting.

4.2.4 Fluid-saturated and precondtioned aluminous metapelite

The calculated behaviour of the fluid-saturated and preconditioned metapelite compositions with the various I-type magma fluid sources at 4 kbar and 750 °C is shown in Figure 4.6a and b. Similar to the metagreywacke, a low-H_2O magma is not capable of inducing melting in this composition. Progressive melting is calculated to have a much smaller effect on μ_{H_2O} in the metapelite than in other compositions, and even 40 mol% melt leads to an almost negligble change of μ_{H_2O} (Fig. 4.6). Consequently, both the typical and high-H_2O magma compositions induce in excess of 50 mol.% melting in the fluid-saturated metapelite, whereas the preconditioned metapelite is only moderately less fertile, yielding ∼45 mol.% melt from interaction with a typical I-type magma (Fig. 4.6).

Chapter 5

Comparison of modelling results with documented case studies

5.1 Composite grey gneiss complexes

The key features of diffusively-fluxed melting as documented in composite grey gneisses are faithfully reproduced in the modelling results, including the persistence of hydrous phases like biotite and the preferential consumption of K-feldspar along with plagioclase and quartz during melting (Collins *et al.*, 1989; Mogk, 1992; Pognante, 1992; Nédélec *et al.*, 1993; Sawyer, 1998; Escuder Viruete, 1999; Jung *et al.*, 2000; White *et al.*, 2005; Jung *et al.*, 2009; Sawyer, 2010; Lee & Cho, 2013; Finch *et al.*, 2014; Carvalho *et al.*, 2016; Wu *et al.*, 2018). Compared to the selected case studies, the protolith assemblage predicted for the modelled average composite grey gneiss compositions is representative and consists predominantly of plagioclase and quartz with minor abundances of biotite and alkali feldspar. A minor discrepancy is the trace amounts of augite predicted by the modelling for the tonalitic grey gneiss composition (Fig. 4.1a, c), which is not observed in the Opatica protolith. However, the amount of augite is negligible (1–2 mol.%) and neither its presence nor absence affects the melting process being described in this thesis.

The T-M_{H_2O} modelling estimates that there is insufficient K-feldspar in both average composite grey gneiss compositions to produce the quantities of melt observed in the Opatica and Kinawa migmatites (Fig. 4.1). This is expected given the lower K_2O content of both average composite grey gneiss compositions compared to those of the case studies (Table 3.1). Despite this, the maximum amounts of melt estimated by Sawyer (2010) for the Opatica Subprovince (25–30 mol.%) and Carvalho *et al.* (2016) for the Kinawa migmatites (35–40 mol.%) are reproduced in the modelling at or around the conditions where K-feldspar is exhausted. The modelling also suggests that after these aforementioned melting events, the residuum composition for the tonalitic grey gneiss and TTG grey gneiss are either K-feldspar absent or severely K-feldspar depleted. This is corroborated by the case studies, where the residual

rocks of the Opatica are mostly K-feldspar absent, whereas the Kinawa residual rocks are K-feldspar-depleted (Sawyer, 2010; Carvalho *et al.*, 2016).

The diffusively-fluxed melting reactions for both average composite grey gneiss compositions, and the approximate proportions of reactants and products normalised to consume 1 mol.% H_2O, are estimated by the modelling results to initially be

$$1.7\ \text{K}-\text{feldspar} + 1.6\ \text{plagioclase} + 1.5\ \text{quartz} \pm 0.1\ \text{biotite} + 1.0\ H_2O = 5.0\ \text{melt} \quad (5.1)$$

for the initial melting interval until K-feldspar is consumed, following which the reaction becomes

$$2.5\ \text{plagioclase} + 1.3\ \text{quartz} \pm 0.3\ \text{biotite} + 1.0\ H_2O = 4.1\ \text{melt}. \quad (5.2)$$

Sawyer (2010) assumes K-feldspar is the limiting reactant during melting in the Opatica Subprovince and to estimate the amount of melt produced (25–30 mol.%), Sawyer (2010) used the average K-feldspar content (9.4 mol.%) of the protolith in mass balance calculations. With 9.4 mol.% K-feldspar, the diffusively-fluxed melting reaction from the modelling results predicts 28.2% partial melting and this is in agreement with Sawyer (2010). Similarly, Carvalho *et al.* (2016) suggests that the Kinawa migmatites could have undergone 60% partial melting if the maximum amount of K-feldspar (20 mol.%) available was entirely consumed, and the modelling results corroborate these estimates. However, geochemical modelling of the Kinawa migmatites suggests that these rocks only yielded 35–40 mol.% melt, suggesting that the melting reaction did not proceed to exhaustion of K-feldspar (Carvalho *et al.*, 2016). If the availability of H_2O is not considered to be a limiting factor for melting in the Opatica Subprovince and Kinawa migmatites (Sawyer, 2010; Carvalho *et al.*, 2016), the modelling indicates that the melting process respectively required 5.6–6.8 and 7–8.2 mol.% H_2O to have been freely available and easily accessible to these target lithologies.

5.2 Metagreywackes

Calculations from the T-M_{H_2O} modelling reproduce the salient features described in examples from metagreywackes, including the preferential consumption of plagioclase and quartz during melting and the relative stability of hydrous phases like biotite (Fig. 4.2; Milord *et al.*, 2001; Fornelli *et al.*, 2002; Genier *et al.*, 2008; Schwindinger & Weinberg, 2017). The presence of other P–T dependent phases such as sillimanite, K-feldspar and garnet are appropriately replicated for metagreywackes at these considered conditions. The range in melt volume (10–40 mol.%) estimated by the various examples considered, is also easily reproduced in the modelling. To yield an approximated average of 20 mol.% melt in the metagreywacke, an

influx of 3.8 mol.% H_2O is required.

The modelling results estimate the diffusively-fluxed melting reactions for the metagreywacke, and the approximate stoichiometry of reactants and products, to initially be

$$2.1\ \text{plagioclase} + 2.6\ \text{quartz} + 1.1\ \text{sillimanite} + 1.7\ \text{biotite} + 1.0\ H_2O = 5.3\ \text{melt} + 2.0\ \text{cordierite} \pm 0.1\ \text{garnet} \tag{5.3}$$

until sillimanite is consumed, following which the reaction becomes

$$2.1\ \text{plagioclase} + 1.7\ \text{quartz} + 0.3\ \text{cordierite} + 0.7\ \text{biotite} + 1.0\ H_2O = 3.6\ \text{melt} + 0.3\ \text{garnet}. \tag{5.4}$$

These melting reactions predominantly consume plagioclase and quartz, similar to the proposed melting reactions taken from various metagreywacke examples (reactions 2.1 and 2.2; Milord *et al.*, 2001; Fornelli *et al.*, 2002; Genier *et al.*, 2008; Schwindinger & Weinberg, 2017). There is a discrepancy between the calculated reactions above and the real-world examples in that the calculated reactions predict minor biotite, sillimanite and cordierite as additional reactants, whereas the natural examples document the consumption of muscovite and K-feldspar. This can most likely be attributed to the selected bulk composition and P–T conditions for the modelling which are representative for this rock type but unsuitable for detailed comparison with one or more of the natural examples considered. Importantly, these minor differences do not affect the general melting process being described here.

5.3 Low-pressure aluminous metapelites

The modelling results reproduce key features of diffusively-fluxed melting as reported in low-pressure metapelitic terranes, including the presence of cordierite, the persistence of hydrous phases like biotite as well as the preferential consumption of K-feldspar, quartz and plagioclase during melting (Wickham & Taylor, 1985; Wickham, 1987; Yardley & Barber, 1991; Ellis & Obata, 1992; Cartwright *et al.*, 1995; Cartwright & Buick, 1998; Genier *et al.*, 2008; Ward *et al.*, 2008; Kisters *et al.*, 2009). A nominally anhydrous phase like garnet, which is documented in the Kuiseb Schists, is absent at the conditions considered for the modelling (Fig. 4.3a). However it is likely to have been introduced either by slightly higher melting temperatures as shown in the modelling or by other open-system diffuse processes (e.g. White *et al.*, 2004), which cannot be reproduced in this diagram. Despite this discrepancy, the modelling results are consistent with the observed mineralogy and features associated with in-situ partial melting in the Kuiseb Schists (Ward *et al.*, 2008).

The modelling also reproduces the maximum amount of melt estimated by Ward *et al.* (2008) for the Kuiseb Schists (10 mol.%), requiring an influx of only 2 mol.% H_2O. The

residuum assemblage calculated by the modelling after 10% partial melting is consistent with the cordierite-bearing residual rocks of the Kuiseb Schist, which are noted to be poor in K-feldspar and depleted in quartz and plagioclase (Ward *et al.*, 2008).

The diffusively-fluxed melting reactions for the aluminous metapelite, and the approximate mole proportions of reactants and products, are estimated to initially be

$$2.8\ \text{K}-\text{feldspar} + 0.7\ \text{plagioclase} + 1.8\ \text{quartz} + 0.6\ \text{cordierite} + 1.0\ \text{H}_2\text{O} = 5.9\ \text{melt} \pm 0.1\ \text{biotite} \tag{5.5}$$

until quartz is consumed, following which the reaction becomes

$$2.4\ \text{K}-\text{feldspar} + 0.7\ \text{plagioclase} + 0.9\ \text{cordierite} + 1.0\ \text{H}_2\text{O} = 3.6\ \text{melt} + 0.5\ \text{biotite}. \tag{5.6}$$

A notable difference between the results of the modelling and the described examples is that the modelling indicates that cordierite is consumed as a reagent by the melting reaction, whereas the growth of new cordierite is documented in most case studies (Weinberg & Hasalová, 2015). One other difference is that the experimentally-determined melting reaction proposed for the Kuiseb Schists (reaction 2.3; Ward *et al.*, 2008) has biotite as a reagent, whereas the modelling indicates that biotite is a minor product of the melting reaction.

Chapter 6

Discussion

6.1 What is the actual melting process?

Throughout this thesis, the process being described has been referred to as 'diffusively-fluxed melting' whereas others have mostly referred to it as 'water-fluxed melting' (e.g. Milord *et al.*, 2001; Sawyer, 2010; Weinberg & Hasalová, 2015; Collins *et al.*, 2016; Weinberg, 2016; Schwindinger & Weinberg, 2017). Weinberg & Hasalová (2015) define water-fluxed melting as synonymous with water-assisted or water-present melting and state that it describes "crustal melting (in) the presence of a free H_2O phase", a definition commonly associated with the more conventional term of fluid-present melting. Other case studies also envisage water-fluxed melting to occur in the presence of free water, even at suprasolidus conditions, such that it is clearly a defining characteristic of the term (e.g. Cartwright & Buick, 1998; Jung *et al.*, 2000; Fornelli *et al.*, 2002; Slagstad *et al.*, 2005; Jung *et al.*, 2009; Lee & Cho, 2013; Dubinina *et al.*, 2015). The alternative to this is dehydration or fluid-absent melting, where "water is supplied by the breakdown of hydrous minerals" (Weinberg & Hasalová, 2015).

The process investigated here is the former, as it involves melting by the addition of H_2O, but the modelling results clearly show that melting does not occur in the presence of a physically-distinct and mechanically separable free water phase at any point. This is a notable departure from water-fluxed melting as it is defined, and therefore requires a more appropriate terminology. I propose diffusively-fluxed melting to be a better description of the process because it still indicates that melting is due to the ingress of an external agent, but emphasises that the movement is diffusive rather than mechanical. This also implies that the agent is not present as a distinct and mechanically separable phase during the process. In this context, water-fluxed melting may be considered as a special case of diffusively-fluxed melting, where diffusively-fluxed melting can occur at any a_{H_2O}, whereas water-fluxed melting only occurs at $a_{H_2O} = 1$. Similarly, diffusively-fluxed melting could conceivably be driven by flux of any highly mobile melt-inducing element, such as H_2O, K_2O or Na_2O, whereas water-fluxed melting—and the example of diffusively-fluxed melting described here—only considers H_2O.

The modelling calculations show that the only conditions where melt coexists with a free water phase is at the wet solidus, and even geologically unrealistic amounts of H_2O fluxed into a bulk composition does not meaningfully expand the realm of fluid-present melting from these very specific P–T conditions (Figs. 4.1–4.3). This is inconsistent with inferences of water-present melting occurring at higher-temperature suprasolidus conditions (Jung *et al.*, 2000, 2009; Lee & Cho, 2013; Slagstad *et al.*, 2005; Cartwright & Buick, 1998; Fornelli *et al.*, 2002; Dubinina *et al.*, 2015; Weinberg & Hasalová, 2015; Collins *et al.*, 2016). One explanation for allowing free water at suprasolidus conditions involves rapid, out-of-equilibrium transport along fractures or shear zones (e.g. Weinberg & Hasalová, 2015), but the calculations show that even extreme volumes of H_2O will only cause more wet solidus melting and not penetrate to higher suprasolidus temperatures (Figs. 4.1–4.3). In all compositions, melting is inferred from the natural examples to have occurred at temperatures that are at least 30–50 °C higher than the wet solidus, and at a_{H_2O} significantly lower than unity or $a_{H_2O} = 1$ (Figs. 4.1–4.3).

The suggested model for how this melting process occurs is that an H_2O-bearing but H_2O-undersaturated magma mechanically migrates into or through the suprasolidus target rocks at these conditions. Although the magma is rising through the crust, the H_2O content is too low for the magma to become H_2O-saturated and undergo degassing (cf. Plank *et al.*, 2013; Collins *et al.*, 2016). Because the magma has higher a_{H_2O} / μ_{H_2O} than the target rocks (Figs. 4.5; 4.6), a chemical potential gradient develops that allows diffusional interaction between the magma and the target rocks, with H_2O diffusing from the magma into the target rocks. The process is exactly the same as described by White & Powell (2010) for crystallising leucosome. However, here the exchange of H_2O leads to melting of the target rocks, and is coupled to the crystallisation of anhydrous minerals in the source magma. For a situation where the process occurs next to a magma conduit, continuous replenishment by fresh magma batches will allow melting of the target rocks to continue until the chemical potentials of the magma and target rocks are equalised. However, for a situation where the process occurs next to an emplaced magma, the process may also be limited by the amount of H_2O that the magma can release before it solidifies. Both these situations are explored in more detail below.

6.2 Requirements and limitations imposed by the target rocks

The modelling calculations indicate that diffusively-fluxed melting of common crustal lithologies can produce melt volumes comparable to those produced by dehydration melting reactions in quartzofeldspathic rocks over a range of P–T conditions. The process does not appear to be restricted to specific rock types, mineral assemblages, H_2O contents or P–T conditions, but can proceed for as long as H_2O is readily available.

6.2.1 Mineralogy and melting reactions

Irrespective of the mineralogy of the different target lithologies considered here, the modelled melting reactions all have a similar form and principally consume feldspars and quartz, consistent with the melting reactions constrained from case studies. Where both K-feldspar and plagioclase are present, these are consumed in approximately equal proportions (e.g. reaction 5.1), but if K-feldspar is absent or becomes exhausted, plagioclase becomes a principal reagent (reactions 5.2, 5.3 & 5.4). Biotite does not have a controlling influence on the melting reaction, and can either be consumed (reactions 5.1–5.4) or produced (reaction 5.6) in minor amounts during melting (e.g. Sawyer, 2010; Carvalho *et al.*, 2016; Weinberg & Hasalová, 2015). The minor discrepancies noted in Section 5 between the calculated reactions and the natural examples can be attributed to the use of average compositions and P–T conditions in the modelling. The modelling calculations represent the general behaviour of the lithologies considered and therefore, minor inconsistencies with the selected natural examples are expected, but these do not affect the overall conclusions.

Sawyer (2010) and Carvalho *et al.* (2016) suggested that the consumption of K-feldspar is essential for melting to proceed, such that the amount of K-feldspar in the target rocks effectively controls the maximum amount of melt that can be produced. However, the modelling results show that the presence of K-feldspar in the target rocks is not a prerequisite for melting, and melting can initiate or continue in K-feldspar absent assemblages such as the metagreywacke and composite grey gneiss compositions (Figs. 4.1; 4.2). Melting in the absence of K-feldspar consumes larger amounts of plagioclase to produce liquids that are more tonalitic or trondhjemitic in composition (cf. Patiño Douce & Harris, 1998; Gardien *et al.*, 2000). This has the knock-on effect of the melts also becoming relatively more H_2O-rich (Stuck & Diener, 2018) and raising a_{H_2O} of the target rocks (Figs. 4.1–4.3).

Quartz is the other principal reactant, but is abundant enough that that it is not typically exhausted, even with melting in excess of 50 mol.% (Figs. 4.1–4.3). Quartz does become depleted in the metapelite, and this markedly reduces the rate of melting, indicating that the presence of quartz is required for voluminous and rapid melt production.

6.2.2 Protolith H_2O content and preconditioning

In the calculations it was assumed that all the target lithologies were maximally hydrated at the wet solidus, and carried the maximum amount of H_2O to suprasolidus conditions. This means that different lithologies hold very different H_2O contents, depending on the proportion of hydrous minerals present in the subsolidus assemblage. It was further assumed that this H_2O content was not reduced by melt loss prior to diffusively-fluxed melting. These assumptions would minimise the effectiveness and impact of diffusively-fluxed melting, but a comparison of the melting behaviour of a maximally hydrated and preconditioned metapelite demonstrates that the H_2O content of the protolith does not have a significant influence on

the process in this example. The two compositions behave similarly with the influx of fluids, with both undergoing near identical diffusively-fluxed melting reactions and yielding similar proportions of melt at similar rates. However, a key distinguishing factor is that quartz and K-feldspar are exhausted with 0.5 mol.% less H_2O in the preconditioned metapelite than the fluid-saturated example, due to prior melting slightly depleting these minerals.

I therefore conclude that diffusively-fluxed melting can occur in normally-hydrated compositions, and that it is not restricted to lithologies with low proportions of hydrous minerals. It also does not require anomalously dry compositions, such as may be produced by prior dehydration or melt loss. If anything, earlier melt loss reduces the amount of melt that can be produced, similar to the effect of multiple melt-loss events during progressive dehydration melting (e.g. White & Powell, 2002; Korhonen *et al.*, 2010).

6.2.3 P–T conditions

Examples of diffusively-fluxed melting in the literature suggest that it preferentially occurs at relatively low pressures approximating mid-crustal depths and upper amphibolite-facies temperatures (Weinberg & Hasalová, 2015). The modelling calculations encompassed a P–T range of 2–8 kbar and 700–750 °C (Fig. 4.5a) and indicate that diffusively-fluxed melting can be initiated over a large range of mid-crustal conditions. However, because the μ_{H_2O} gradient between the magma and target lithology increases towards lower pressure (Fig. 4.5a), mid- to upper-crustal conditions would be more favourable for the process, and allow larger volumes of melt to be produced. A notable exception to this is the metagreywacke composition, as its μ_{H_2O} is strongly dependent on pressure, particularly at low melt volumes (Fig. 4.5d). Because of this dependence, diffusively-fluxed melting in the metagreywacke is limited to P below 5.2 kbar at 750 °C (Fig. 4.5d).

Temperature has a secondary influence on the process. The μ_{H_2O} gradient between the magma and target rocks can be seen to increase with temperature (Fig. 4.5a), thereby allowing larger melt volumes to be produced before the gradient is equalised. In general, it is only once melting progresses and μ_{H_2O} of the target rocks increase, that P–T conditions have a significant influence on the process and the potential volume of melt produced.

6.3 Limitations imposed by the fluid source

6.3.1 μ_{H_2O} required for forward flux

The key driving force for diffusively-fluxed melting is a difference in μ_{H_2O} between the source of H_2O and the rock undergoing melting. Consequently, any feature with a high enough μ_{H_2O} could initiate the process and serve as a fluid source. Lithologies with low proportions of hydrous minerals such as the tonalitic grey gneiss and TTG grey gneiss have a low enough μ_{H_2O} prior to melting that even a very dry fluid source, such as a low-H_2O magma with only 5 mol.% H_2O, can trigger melting by forward flux. However, for the metagreywacke and

aluminous metapelite, this dry magma source is insufficient to initiate melting. Unlike the two grey gneiss examples, these more hydrous target lithologies do impose minimum thresholds on the μ_{H_2O} and H_2O content of the fluid source. However, these lithologies do not require anomalously hydrous or unusual fluid sources, and a typical I-type magma with 13 mol.% H_2O is sufficient to initiate and sustain diffusively-fluxed melting for all target lithology types (Fig. 4.5). Given that diffusively-fluxed melting does not appear to require a very specific or unusual fluid source, I conclude that this does not impose a primary limitation on the feasibility or initiation of the process.

μ_{H_2O} does become significant in determining the amount of melt that can be produced from a specific target lithology. In all cases, μ_{H_2O} of the target increases as melting proceeds, and the μ_{H_2O} gradient between the source and target is progressively flattened. The μ_{H_2O} response to melting is not linear for an individual lithology, and is not comparable between different lithologies, such that the amount of melt that can be produced before μ_{H_2O} gradients are equalised is highly variable (Figs. 4.5; 4.6). Once μ_{H_2O} of the target and source are equalised, the driving force for the process is removed, and therefore the μ_{H_2O} of the fluid source provides an absolute maximum limit on the amount of melt that can be generated by diffusively-fluxed melting.

6.3.2 Fluid volume

The previous section demonstrated that typical I-type magmas are a viable fluid source to drive diffusively-fluxed melting. However, thus far I have assumed that the fluid source is infinite, as would be the case if the process was occurring next to a magma conduit. This assumption removed any need to consider H_2O availability as a limiting factor in the process (cf. Sawyer, 2010; Carvalho *et al.*, 2016), or how H_2O flux affects the magma source. The calculations show that the high degrees of melting often reported (more than 30 vol.%, e.g. Butler *et al.*, 1997; Milord *et al.*, 2001; Weinberg & Hasalová, 2015; Carvalho *et al.*, 2016) requires the fluid source to yield 6–8 mol.% H_2O (Figs. 4.1–4.3).

Without the focussing effect of a magma conduit, a typical I-type magma containing 13 mol.% H_2O (4 wt.%; Plank *et al.*, 2013) would have to give up more than half of its H_2O content to achieve this. A comparison of μ_{H_2O} for the typical- and low-H_2O magma indicates that the magma would be capable of doing this, at least for a composite grey gneiss target rock, without equalising μ_{H_2O} gradients (Figs. 4.5b; 4.5c). However, removal of this amount of H_2O from the magma would lead to a dramatic crystallisation of anhydrous minerals. Prior to diffusively-fluxed melting, the typical magma is estimated to have a solid crystal load of 45 mol.% (Fig. 4.4). Removal of 6–8 mol.% H_2O increases this solid load by more than 27–37 mol.% to in excess of 71–81 mol.%. This would push the rheology of the magma over the rheologically critical melt percentage threshold (35–40 vol.% melt; van der Molen & Paterson, 1979; Rosenberg & Handy, 2005) and cause it to transition from a liquid to a solid, effectively arresting its ascent and leading to emplacement.

Therefore, without a focussing mechanism, the amount of melting in the target rock coincides with similar volumes of crystallisation in the magmatic fluid source. Significantly, this does not lead to the net generation of additional melt. Depending on the target lithology, there may be moderate to large compositional differences between the relict source magma and newly-formed melts from the target rock, which may change the overall magma composition through mingling and hybridisation (Schwindinger & Weinberg, 2017). I therefore conclude that, whereas diffusively-fluxed melting can occur around emplaced and crystallising magma bodies (Weinberg & Hasalová, 2015), this amounts to a transference of melt from the crystallising body to the target rocks, and does not generate any additional magma volumes.

6.3.3 Geometry of viable fluid sources

The need for the fluid source to be focussed means that melt conduits are the only viable fluid source, and that diffusively-fluxed melting will ultimately be confined to areas of the crust that are accessible to melt fluxes. Granitic melt migration in the suprasolidus and near-solidus crust initiates in networks of interconnected melt-filled fractures (Collins & Sawyer, 1996; Weinberg, 1999; Leitch & Weinberg, 2002; Weinberg & Regenauer-Lieb, 2010) that coalesce and become more pervasive in areas of high strain, such as shear zone systems (Brown *et al.*, 2011, and references therein). Whereas a pervasive melt network has a high density of melt-bearing structures that provide access to a large target volume, the volume of melt moving along an individual structural element is limited, which will inhibit the effectiveness of diffusively-fluxed melting. A shear zone system can carry much larger volumes of melt and be long-lived, providing the ideal environment for effective diffusively-fluxed melting. This is indeed the exact setting inferred by Carvalho *et al.* (2016), and the preferred setting advocated in the review by Weinberg & Hasalová (2015).

Whereas a large-scale shear zone can easily carry the requisite melt volumes, it is a relatively confined structure that will only affect a limited volume of target rocks that are in close enough proximity to experience diffusivity of H_2O. It is difficult to estimate an exact distance for the diffusivity of H_2O under these conditions, but it is likely to be on the order of a tens of metres (e.g. Austrheim, 1987). From these constraints I conclude that diffusively-fluxed melting will be spatially-restricted and only be possible in areas of the crust that are within narrow envelopes in and around melt-bearing shear zones. This is the main limitation on the viability of the process as a mechanism for large-scale melt generation and crustal differentiation.

6.4 Diffusively-fluxed melting as a mechanism for crustal differentiation

In order for diffusively-fluxed melting to be a process that meaningfully contributes to crustal differentiation, it needs to produce melt volumes comparable to that produced by dehydration melting, and it needs to readily occur in a variety of tectonic environments. In the

previous sections I highlighted that there are no first-order restrictions on the feasibility of diffusively-fluxed melting that are imposed by the target lithologies. My calculations show that, by volume of rock, diffusively-fluxed melting produces similar melt volumes to dehydration melting. These melt fractions are high enough to readily segregate and migrate from their source. Similarly, the fluid source does not need to have any special or unusual characteristics. However, if the fluid source is anything other than a magma conduit, the produced melt will be balanced by crystallisation of a similar fraction of the source magma. Such a scenario only moves an existing melt volume from the source to the target and therefore does not amount to net melt generation. Without a net increase in the volume of melt in the system, I do not consider this process to provide a first-order contribution to crustal differentiation.

Therefore, the main limitation to diffusively-fluxed melting as a mechanism for crustal differentiation is imposed by the availability of suitable magma conduit fluid sources in the near-solidus crust. Melting will be restricted to the areas immediately in and around these structures, as this is the only part of the crust that is diffusively accessible to H_2O. The general dearth of melt conduits in exhumed mid-crustal orogenic terranes (Brown & Solar, 1999; Weinberg, 1999; Kisters *et al.*, 2009; Reichardt & Weinberg, 2012; Brown, 2013) suggests that these structures are not very common. Even assuming a generous 100 m to km-wide H_2O diffusivity envelope around each, this still implies that the volume of crust that can potentially be affected by diffusively-fluxed melting is a very minor portion of the anatectic orogenic crust as a whole. This ultimately limits its effectiveness as a means of crustal differentiation. Dehydration melting occurs in the entire anatectic orogenic crust, and simple economics of scale dictate that it must therefore be the main process by which crustal differentiation occurs. That is not to say that diffusively-fluxed melting is not a locally significant process. In and around melt-bearing shear zones, it can play an important role in raising melt volumes, which would lead to further rheological weakening. Mingling and hybridisation of the new, relatively low-temperature melts with ascending magmas could affect aspects of the magma chemistry, thereby also contributing to the evolution of some granitoids and diversity of granite compositions (Schwindinger & Weinberg, 2017).

In conclusion, diffusively-fluxed melting is a feasible petrogenetic process capable of producing melt volumes comparable to that of dehydration melting for a variety of lithologies and P–T conditions in the lower to mid-continental crust, provided that a suitable magma conduit fluid source is available. However, considering the seemingly insurmountable limitations imposed on this mechanism by the geometry of the fluid source, diffusively-fluxed melting is unlikely to be a general and significant contributor to crustal differentiation.

References

Ague, J. J., 1991. Evidence for major mass transfer and volume strain during regional metamorphism of pelites. *Geology*, **19**, 855–858.

Annen, C. & Sparks, R. S. J., 2002. Effects of repetitive emplacement of basaltic intrusions on thermal evolution and melt generation in the crust. *Earth and Planetary Science Letters*, **203**, 937–955.

Arzi, A., 1978. Critical phenomena in the rheology of partially melted rocks. *Tectonophysics*, **44**, 173–184.

Austrheim, H., 1987. Eclogitization of lower crustal granulites by fluid migration through shear zones. *Earth and Planetary Science Letters*, **81**, 221–232.

Berger, A., Burri, T., Alt-Epping, P. & Engi, M., 2008. Tectonically controlled fluid flow and water-assisted melting in the middle crust: An example from the Central Alps. *Lithos*, **102**, 598–615.

Brown, M., 1979. The petrogenesis of the St. Malo migmatite belt, Armorican Massif, France, with particular reference to the diatexites. *Neues Jahrbuch für Mineralogie—Abhandlungen*, **135**, 48–74.

Brown, M., 2013. Granite: From genesis to emplacement. *Bulletin of the Geological Society of America*, **125**, 1079–1113.

Brown, M. & Korhonen, F. J., 2009. Some remarks on melting and extreme metamorphism of crustal rocks. In: *Physics and Chemistry of the Earth's Interior*, (eds Gupta, A. K. & Dasgupta, S.), New Delhi, pp. 67–88. Springer.

Brown, M. & Solar, G. S., 1999. The mechanism of ascent and emplacement of granite magma during transpression: A syntectonic granite paradigm. *Tectonophysics*, **312**, 1–33.

Brown, M., Korhonen, F. J. & Siddoway, C. S., 2011. Organizing melt flow through the crust. *Elements*, **7**, 261–266.

Butler, R. W. H., Harris, N. B. W. & Whittington, A. G., 1997. Interactions between deformation, magmatism and hydrothermal activity during active crustal thickening: A

field example from Nanga Parbat, Pakistan Himalayas. *Mineralogical Magazine*, **61**, 37–52.

Carlson, W. D., 2002. Scales of disequilibrium and rates of equilibration during metamorphism. *American Mineralogist*, **87**, 185–204.

Cartwright, I. & Buick, I. S., 1998. The link between oxygen isotope resetting, partial melting, and fluid flow in metamorphic terrains. *Terra Nova*, **10**, 81–85.

Cartwright, I., Vry, J. & Sandiford, M., 1995. Changes in stable isotope ratios of metapelites and marbles during regional metamorphism, Mount Lofty Ranges, South Australia: implications for crustal scale fluid flow. *Contributions to Mineralogy and Petrology*, **120**, 292–310.

Carvalho, B. B., Sawyer, E. W. & Janasi, V. A., 2016. Crustal reworking in a shear zone: Transformation of metagranite to migmatite. *Journal of Metamorphic Geology*, **34**, 237–264.

Clemens, J. D., 2006. Melting of the continental crust: fluid regimes, melting reactions, and source-rock fertility. In: *Evolution and Differentiation of the Continental Crust*, (eds Brown, M. & Rushmer, T.), Cambridge, UK, pp. 296–330. Cambridge University Press.

Clemens, J. D. & Droop, G. T. R., 1998. Fluids, P-T paths and the fates of anatectic melts in the Earth's crust. *Lithos*, **44**, 21–36.

Clemens, J. D. & Stevens, G., 2015. Comment on 'Water-fluxed melting of the continental crust: A review' by R.F. Weinberg and P. Hasalová. *Lithos*, **234-235**, 100–101.

Clemens, J. D. & Vielzeuf, D., 1987. Constraints on melting and magma production in the crust. *Earth and Planetary Science Letters*, **86**, 287–306.

Collins, W. J. & Sawyer, E. W., 1996. Pervasive granitoid magma transfer through the lower-middle crust during non-coaxial compressional deformation. *Journal of Metamorphic Geology*, **14**, 565–579.

Collins, W. J., Flood, R. H., Vernon, R. H. & Shaw, S. E., 1989. The Wuluma granite, Arunta Block, central Australia: An example of in situ, near-isochemical granite formation in a granulite-facies terrane. *Lithos*, **23**, 63–83.

Collins, W. J., Huang, H. Q. & Jiang, X., 2016. Water-fluxed crustal melting produces Cordilleran batholiths. *Geology*, **44**, 143–146.

Diener, J. F. A. & Fagereng, Å., 2014. The influence of melting and melt drainage on crustal rheology during orogenesis. *Journal of Geophysical Research: Solid Earth*, **8**, 1–18.

Dubinina, E. O., Aranovich, L. Y., van Reenen, D. D., Avdeenko, A. S., Varlamov, D. A., Shaposhnikov, V. V. & Kurdyukov, E. B., 2015. Involvement of fluids in the metamorphic processes within different zones of the Southern Marginal Zone of the Limpopo complex, South Africa: An oxygen isotope perspective. *Precambrian Research*, **256**, 48–61.

Ellis, D. J. & Obata, M., 1992. Migmatite and melt segregation at Cooma, New South Wales. *Transactions of the Royal Society of Edinburgh: Earth Sciences*, **83**, 95–106.

Escuder Viruete, J., 1999. Hornblende-bearing leucosome development during syn-orogenic crustal extension in the Tormes Gneiss Dome, NW Iberian Massif, Spain. *Lithos*, **46**, 751–772.

Etheridge, M. A., Wall, V. J. & Vernon, R. H., 1983. The role of fluid phase during regional metamorphism and deformation. *Journal of Metamorphic Geology*, **1**, 205–226.

Finch, M., Hasalová, P., Weinberg, R. F. & Fanning, C. M., 2014. Switch from thrusting to normal shearing in the Zanskar shear zone, NW Himalaya: Implications for channel flow. *Bulletin of the Geological Society of America*, **126**, 892–924.

Finger, F. & Clemens, J. D., 1995. Migmatization and "secondary" granitic magmas: effects of emplacement and crystallization of "primary" granitoids in Southern Bohemia, Austria. *Contributions to Mineralogy and Petrology*, **120**, 311–326.

Fornelli, A., Piccareta, G., Del Moro, A. & Acquafredda, P., 2002. Multi-stage melting in the lower crust of the Serre (Southern Italy). *Journal of Petrology*, **43**, 2191–2217.

Garde, A. A., 1997. *Accretion and evolution of an Archaean high-grade grey gneiss – amphibolite complex: the Fiskefjord area, southern West Greenland*, Vol. 177, Geological Survey of Denmark and Greenland.

Gardien, V., Thompson, A. B. & Ulmer, P., 2000. Melting of biotite + plagioclase + quartz gneisses: the role of H_2O in the stability of amphibole. *Journal of Petrology*, **41**, 651–666.

Genier, F., Bussy, F., Epard, J. L. & Baumgartner, L., 2008. Water-assisted migmatization of metagraywackes in a Variscan shear zone, Aiguilles-Rouges massif, western Alps. *Lithos*, **102**, 575–597.

Green, E. C. R., White, R. W., Diener, J. F. A., Powell, R., Holland, T. J. B. & Palin, R. M., 2016. Activity-composition relations for the calculation of partial melting equilibria in metabasic rocks. *Journal of Metamorphic Geology*, **34**, 845–869.

Hasalová, P., Štípská, P., Powell, R., Schulmann, K., Janoušek, V. & Lexa, O., 2008. Transforming mylonitic metagranite by open-system interactions during melt flow. *Journal of Metamorphic Geology*, **26**, 55–80.

Heinrich, C. A., 1982. Kyanite-eclogite to amphibolite fades evolution of hydrous mafic and pelitic rocks, Adula nappe, Central Alps. *Contributions to Mineralogy and Petrology*, **81**, 30–38.

Hoernes, S. & Friedrichsen, H., 1978. Oxygen and hydrogen isotope study of the polymetamorphic area of the northern Otztal-Stubai Alps (Tyrol). *Contributions to Mineralogy and Petrology*, **67**, 305–315.

Holk, G. J. & Taylor, H. P., 1997. $^{18}O/^{16}O$ homogenization of the middle crust during anatexis: The Thor-Odin metamorphic core complex, British Columbia. *Geology*, **25**, 31–34.

Holk, G. J. & Taylor, H. P., 2000. Water as a petrologic catalyst driving $^{18}O/^{16}O$ homogenization and anatexis of the middle crust in the metamorphic core complexes of British Columbia. *International Geology Review*, **42**, 97–130.

Holland, T. J. B. & Powell, R., 2011. An improved and extended internally consistent thermodynamic dataset for phases of petrological interest, involving a new equation of state for solids. *Journal of Metamorphic Geology*, **29**, 333–383.

Huppert, H. E. & Sparks, R. S. J., 1988. The generation of granitic magmas by intrusion of basalt into continental crust. *Journal of Petrology*, **29**, 599–624.

Johannes, W. & Holtz, F., 1996. Petrogenesis and Experimental Petrology of Granitic Rocks, *Minerals and Rocks Series*, Vol. 22, Berlin, 335. Springer-Verlag.

Jung, C., Jung, S., Nebel, O., Hellebrand, E., Masberg, P. & Hoffer, E., 2009. Fluid-present melting of meta-igneous rocks and the generation of leucogranites — Constraints from garnet major- and trace element data, Lu-Hf whole rock-garnet ages and whole rock Nd-Sr-Hf-O isotope data. *Lithos*, **111**, 220–235.

Jung, S., Hoernes, S. & Mezger, K., 2000. Geochronology and petrology of migmatites from the Proterozoic Damara Belt — importance of episodic fluid-present disequilibrium melting and consequences for granite petrology. *Lithos*, **51**, 153–179.

Kisters, A. F. M., Ward, R. A., Anthonissen, C. J. & Vietze, M. E., 2009. Melt segregation and far-field melt transfer in the mid-crust. *Journal of the Geological Society*, **166**, 905–918.

Korhonen, F. J., Saito, S., Brown, M. & Siddoway, C. S., 2010. Modeling multiple melt loss events in the evolution of an active continental margin. *Lithos*, **116**, 230–248.

Korzhinskiĭ, D. S., 1959. *Physicochemical Basis of the Analysis of the Paragenesis of Minerals*, Consultants Bureau, New York, NY.

Le Fort, P., Cuney, M., Deniel, C., France-Lanord, C., Sheppard, S., Upreti, B. & Vidal, P., 1987. Crustal generation of the Himalayan leucogranites. *Tectonophysics*, **134**, 39–57.

Lee, Y. & Cho, M., 2013. Fluid-present disequilibrium melting in Neoarchean arc-related migmatites of Daeijak Island, western Gyeonggi Massif, Korea. *Lithos*, **179**, 249–262.

Leitch, A. M. & Weinberg, R. F., 2002. Modelling granite migration by mesoscale pervasive flow. *Earth and Planetary Science Letters*, **200**, 131–146.

Milord, I., Sawyer, E. W. & Brown, M., 2001. Formation of diatexite migmatite and granite magma during anatexis of semi-pelitic metasedimentary rocks: An example from St. Malo, France. *Journal Of Petrology*, **42**, 487–505.

Mogk, D. W., 1992. Ductile shearing and migmatization at midcrustal levels in an Archean high-grade gneiss belt, northern Gallatin range, Montana, USA. *Journal of Metamorphic Geology*, **10**, 427–438.

Moyen, J. F., 2011. The composite Archaean grey gneisses: Petrological significance, and evidence for a non-unique tectonic setting for Archaean crustal growth. *Lithos*, **123**, 21–36.

Münster, A., 1970. *Classical thermodynamics*, Wiley-Interscience, London.

Nédélec, A., Minyem, D. & Barbey, P., 1993. High-P-high-T anatexis of Archaean tonalitic grey gneisses: the Eseka migmatites, Cameroon. *Precambrian Research*, **62**, 191–205.

Norris, R. J. & Henley, R. W., 1976. Dewatering of a metamorphic pile. *Geology*, **4**, 333–336.

Palin, R. M., White, R. W., Green, E. C. R., Diener, J. F. A., Powell, R. & Holland, T. J. B., 2016. High-grade metamorphism and partial melting of basic and intermediate rocks. *Journal of Metamorphic Geology*, **34**, 871–892.

Patiño Douce, A. E. & Harris, N., 1998. Experimental constraints on Himalayan anatexis. *Journal of Petrology*, **39**, 689–710.

Pettijohn, F. J., 1963. Chemical composition of sandstones, excluding carbonate and volcanic sands, *Data of geochemistry*, 6 edn, chapter S, pp. S1–S21.

Plank, T., Kelley, K. A., Zimmer, M. M., Hauri, E. H. & Wallace, P. J., 2013. Why do mafic arc magmas contain ∼4wt% water on average? *Earth and Planetary Science Letters*, **364**, 168–179.

Pognante, U., 1992. Migmatites and leucogranites of Tertiary age from the High Himalayan Crystallines of Zanskar (NW India): a case history of anatexis of Palaeozoic orthogneisses. *Mineralogy and Petrology*, **46**, 291–313.

Powell, R., 1983. Processes in granulite-facies metamorphism. In: *Migmatites, Melting and Metamorphism*, (eds Atherton, M. P. & Gibble, C. D.), pp. 127–139. Shiva, Cheshire.

Powell, R. & Holland, T., 2008. On thermobarometry. *Journal of Metamorphic Geology*, **26**(2), 155–179.

Powell, R. & Holland, T. J. B., 1988. An internally consistent dataset with uncertainties and correlations: 3. Applications to geobarometry, worked examples and a computer program. *Journal of Metamorphic Geology*, **6**, 173–204.

Ramberg, H., 1952. *The Origin of Metamorphic and Metasomatic Rocks: A treatise on recrystallization and replacement in the earth's crust*, University of Chicago Press.

Reichardt, H. & Weinberg, R. F., 2012. Hornblende chemistry in meta- and diatexites and its retention in the source of leucogranites: An example from the Karakoram shear Zone, NW india. *Journal of Petrology*, **53**, 1287–1318.

Rosenberg, C. L. & Handy, M. R., 2005. Experimental deformation of partially melted granite revisited: Implications for the continental crust. *Journal of Metamorphic Geology*, **23**, 19–28.

Rubie, D. C., 1986. The catalysis of mineral reactions by water and restrictions on the presence of aqueous fluid during metamorphism. *Mineralogical Magazine*, **50**, 399–415.

Sandiford, M. & McLaren, S., 2002. Tectonic feedback and the ordering of heat producing elements within the continental lithosphere. *Earth and Planetary Science Letters*, **204**, 133–150.

Sawyer, E. W., 1998. Formation and evolution of granite magmas during crustal reworking: the significance of diatexites. *Journal of Petrology*, **39**, 1147–1167.

Sawyer, E. W., 2010. Migmatites formed by water-fluxed partial melting of a leucogranodiorite protolith: Microstructures in the residual rocks and source of the fluid. *Lithos*, **116**, 273–286.

Schwindinger, M. & Weinberg, R. F., 2017. A felsic MASH zone of crustal magmas — Feedback between granite magma intrusion and in situ crustal anatexis. *Lithos*, **284-285**, 109–121.

Slagstad, T., Jamieson, R. & Culshaw, N., 2005. Formation, crystallization, and migration of melt in the mid-orogenic crust: Muskoka domain migmatites, Grenville Province, Ontario. *Journal of Petrology*, **46**, 893–919.

Spear, F., Kohn, M. & Cheney, J., 1999. *P–T* paths from anatectic pelites. *Contributions to Mineralogy and Petrology*, **134**, 17–32.

Stevens, G. & Clemens, J. D., 1993. Fluid-absent melting and the roles of fluids in the lithosphere: a slanted summary? *Chemical Geology*, **108**, 1–17.

Stuck, T. J. & Diener, J. F. A., 2018. Mineral equilibria constraints on open-system melting in metamafic compositions. *Journal of Metamorphic Geology*, **36**, 255–281.

Thompson, A. B., 1983. Fluid-absent metamorphism. *Journal of the Geological Society*, **140**, 533–547.

Thompson, J. B., 1955. The thermodynamic basis for the mineral facies concept. *American Journal of Science*, **253**, 65–103.

Turner, F., 1981. *Metamorphic Petrology: Mineralogical, Field, and Tectonic Aspects*, 2 edn, McGraw-Hill Book Company, Hemisphere Publishing Corporation, New York.

Tuttle, O. F. & Bowen, N., 1958. Origin of granite in the light of experimental studies in the system $NaAlSi_3O_8$–$KAlSi_3O_8$–SiO_2–H_2O. *Memoir of the Geological Society of America*, **74**, 1–145.

van der Molen, I. & Paterson, M. S., 1979. Experimental deformation of partially-melted granite. *Contributions to Mineralogy and Petrology*, **70**, 299–318.

Vernon, R. H. & Clarke, G. L., 2008. *Principles of Metamorphic Petrology*, Cambridge University Press, New York.

Wallace, P. J., 2005. Volatiles in subduction zone magmas: Concentrations and fluxes based on melt inclusion and volcanic gas data. *Journal of Volcanology and Geothermal Research*, **140**, 217–240.

Walther, J. V. & Orville, P. M., 1982. Volatile production and transport in regional metamorphism. *Contributions to Mineralogy and Petrology*, **79**, 252–257.

Ward, R., Stevens, G. & Kisters, A., 2008. Fluid and deformation induced partial melting and melt volumes in low-temperature granulite-facies metasediments, Damara Belt, Namibia. *Lithos*, **105**, 253–271.

Webb, G., Powell, R. & McLaren, S., 2015. Phase equilibria constraints on the melt fertility of crustal rocks: the effect of subsolidus water loss. *Journal of Metamorphic Geology*, **33**(2), 147–165.
URL: *https://onlinelibrary.wiley.com/doi/abs/10.1111/jmg.12114*

Weinberg, R. F., 1999. Mesoscale pervasive felsic magma migration: Alternatives to dyking. *Lithos*, **46**, 393–410.

Weinberg, R. F., 2016. Himalayan leucogranites and migmatites: nature, timing and duration of anatexis. *Journal of Metamorphic Geology*, **34**, 821–843.

Weinberg, R. F. & Hasalová, P., 2015. Water-fluxed melting of the continental crust: A review. *Lithos*, **212-215**, 158–188.

Weinberg, R. F. & Regenauer-Lieb, K., 2010. Ductile fractures and magma migration from source. *Geology*, **38**, 363–366.

Whalen, J. B., Currie, K. L. & Chappell, B. W., 1987. A-type granites: geochemical characteristics, discriminations and petrogenesis. *Contributions to Mineralogy and Petrology*, **95**, 407–419.

White, R. W. & Powell, R., 2002. Melt loss and the preservation of granulite facies mineral assemblages. *Journal of Metamorphic Geology*, **20**, 621–632.

White, R. W. & Powell, R., 2010. Retrograde melt-residue interaction and the formation of near-anhydrous leucosomes in migmatites. *Journal of Metamorphic Geology*, **28**, 579–597.

White, R. W., Palin, R. M. & Green, E. C. R., 2017. High-grade metamorphism and partial melting in Archean composite grey gneiss complexes. *Journal of Metamorphic Geology*, **35**, 181–195.

White, R. W., Pomroy, N. E. & Powell, R., 2005. An in situ metatexite-diatexite transition in upper amphibolite facies rocks from Broken Hill, Australia. *Journal of Metamorphic Geology*, **23**, 579–602.

White, R. W., Powell, R. & Halpin, J. A., 2004. Spatially-focussed melt formation in aluminous metapelites from Broken Hill, Australia. *Journal of Metamorphic Geology*, **22**, 825–845.

White, R. W., Powell, R. & Holland, T. J. B., 2001. Calculation of partial melting equilibria in the system Na_2O-CaO-K_2O-FeO-MgO-Al_2O_3-SiO_2-H_2O (NCKFMASH). *Journal of Metamorphic Geology*, **19**, 139–153.

White, R. W., Powell, R. & Johnson, T. E., 2014. The effect of Mn on mineral stability in metapelites revisited: new a-x relations for manganese-bearing minerals. *Journal of Metamorphic Geology*, **32**, 809–828.

White, R. W., Powell, R., Holland, T. J. B., Johnson, T. E. & Green, E. C. R., 2014. New mineral activity-composition relations for thermodynamic calculations in metapelitic systems. *Journal of Metamorphic Geology*, **32**, 261–286.

Wickham, S. M., 1987. The segregation and emplacement of granitic magma. *Journal of the Geological Society, London*, **144**, 281–297.

Wickham, S. M. & Taylor, H. P., 1985. Stable isotopic evidence for large-scale seawater infiltration in a regional metamorphic terrane; the Trois Seigneurs Massif, Pyrenees, France. *Contributions to Mineralogy and Petrology*, **91**, 122–137.

Wu, K., Ling, M. X., Hu, Y. B., Guo, J., Jiang, X. Y., Sun, S. J., Liang, H. Y., Liu, X. & Sun, W., 2018. Melt-fluxed melting of the heterogeneously mixed lower arc crust: A case study from the Qinling Orogenic Belt, Central China. *Geochemistry, Geophysics, Geosystems*, **19**, 1767–1788.

Wyllie, P. J., 1977. Crustal anatexis: An experimental review. *Tectonophysics*, **43**, 41–71.

Yakymchuk, C. & Brown, M., 2014. Consequences of open-system melting in tectonics. *Journal of the Geological Society*, **171**, 21–40.

Yardley, B. W. D., 2009. The role of water in the evolution of the continental crust. *Journal of the Geological Society, London*, **166**, 585–600.

Yardley, B. W. D. & Baltatzis, E., 1985. Retrogression of staurolite schists and the sources of infiltrating fluids during metamorphism. *Contributions to Mineralogy and Petrology*, **89**, 59–68.

Yardley, B. W. D. & Barber, J. P., 1991. Melting reactions in the Connemara Schists: the role of water infiltration in the formation of amphibolite facies migmatites. *American Mineralogist*, **76**, 848–856.

Yardley, B. W. D. & Valley, J. W., 1997. The petrologic case for a dry lower crust. *Journal of Geophysical Research*, **102**, 12173–12185.